Using Directional Entropic Forces
For Target Pattern Design

by

Pablo Souza

A dissertation submitted in partial fulfillment
of the requirements for the degree of
Doctor of Philosophy
(Applied Physics)
in The University of Michigan
2015

Doctoral Committee:

       Professor Sharon C. Glotzer, Chair
       Research Investigator Michael Markus Engel
       Professor Mark E. Newman
       Professor Michael J. Solomon
       Professor Robert M. Ziff

They did not know it was impossible so they did it.

— Mark Twain

À *Tezinha, à Baixinha* e ao *da Flauta*.

Acknowledgments

It is a big understatement to say how impossible it would have been to get this far without help.

Mentors, I had several: from outside (Bob Ziff, Mike Solomon, Nick Kotov, Mark Newman, John Holland) and within the lab (Aaron(s), Ben, Daphne, Greg, Irrgang, Josh, Matt, Michael) – thank you for the lessons and patience.

Friends (Alex, Dimitri, Kee, Hiram, Michelle, Paul, Pedro and many others!!): you are awesome.

Ashley, Karla, Mirtes and Noah-the-bowl-cut: thank you for caring.
Tony, Natercia Damasceno: thanks for believing.

I also thank FAPESP for funding my (interrupted) PhD degree in Brazil and José Pedro Rino for the mentorship. I also thank the important tech that allowed this research to happen: Stack Exchange, Wikipedia, and Wolfram research.

Huge thanks to Karen – the gears running in the lab's background.

Sharon: you (literally) brought me here. I am forever indebted to you.

Table of Contents

List of Tables

List of Figures

Abstract

Designing attributes of a material's building blocks in order to assemble them into a target structure is a major goal in materials science. In this thesis, I present three works exploring the role of geometry for self-assembly of anisotropic Brownian particles. The first work represents a systematic study of the assembly behavior of corner-truncated tetrahedra, leading to the discovery of new crystalline phases. This work also hinted to the possibility that face-to-face contacts between neighboring particles – as a consequence of what we then defined *directional entropic forces* – could lead to a general mechanism explaining entropy-driven assembly of convex hard polyhedra. The study of densest packings of those shapes, also performed in that work, revealed a complex landscape that opened doors for subsequent explorations of the relationship between shape and packing. The second work demonstrates how directional entropic forces can be used to predictively assemble a plethora of hard convex polyhedra into crystalline, quasicrystalline, liquid- and plastic-crystalline structures of unprecedented complexity. This work served not only as a roadmap for many experiments being now performed in the nanoscale but also as a framework from which new assembly strategies could be devised. Finally, the third work shows how the concepts elucidated in those previous works can be used for the assembly of a novel chiral crystalline structure with *a priori* choice of handedness. It also exemplifies the connection between geometry and isotropic interactions that can be used for assembly of complex crystalline and quasicrystalline structures. As a whole, this thesis explores the use of entropic forces as a tool for controllable assembly of stochastic building blocks and it demonstrates how harnessing geometry can have profound impact for the generation of new materials through target pattern design.

Chapter 1

Introduction

There's no need to build a labyrinth when the entire universe is one.
Jorge Luis Borges

The significance of geometry for our understanding of how Nature works has a long scientific history. To Plato, this relationship was so strong that he associated, to each of the 3-dimensional regular solids, the classic elements [1]. And so influential were those ideas that, more than 19 centuries later, the same building blocks were used by Kepler in his design of planetary orbits [2].

In crystallography, the importance of geometry has also come a long way. From the Greeks – who confusedly named clear pieces of solid quartz "krystallos" (meaning *ice*), after believing them to be water solidified in the cold center of mountains [3] – today we arrived at a time when imaging techniques with near-atomistic precision are enabling researchers to unveil complex – and sometimes curious – natural mechanisms such as the ability of chilli peppers to wedge open intricate molecular ion channels in your tongue, resulting on the "fire" sensation similar to that of hot food [4].

This progress in our understanding of the structure of matter is largely due to a "molecular architecture" revolution that can be argued [5] to have started in 1874 with a postulate by van't Hoff proposing that the four valence bonds of the carbon atom were arranged in the corners of a regular tetrahedron. Despite its simplicity, this postulate remained mostly discredited until 40 years later, when the Braggs reported their discovery of the diamond crystal structure [6]. Subsequent discoveries – led largely by Pauling himself – strengthened so much the relationship between geometry and chemical organization that later he argued that the structure of many crystals and molecules could be "conveniently described by reference to the five regular polyhedra" [5]. And the excitement of the newly

discovered double-helix structure instigated him to speculate that "the simplicity of the explanation of the self-duplicating property of DNA (…) gives a basis for hope that additional studies in the field of the molecular architecture of living organisms will lead ultimately to a thorough and satisfying understanding of all of the phenomena of life" [5].

Although this dream has yet to become reality, today we are witnessing an important chapter in this molecular architecture revolution, one in which geometry is departing from being a passive theoretical method, able to help us understand the organization of Nature, towards becoming an active, essential tool that allows tailoring building blocks and their interactions for the design of a new class of target materials. *Shape* is, only now, being explored as a knob for self-assembly. And the consequences of this exploration have just begun to be unveiled.

The work presented in this thesis largely concerns the study of a somewhat restricted class of "molecular architecture": that of convex objects able to organize themselves through Brownian motion into lattices as a result of purely excluded volume interactions. Like Pauling's regular solids, however, the simplicity and universality of those concepts have been demonstrated to have far reaching implications, serving not only as a roadmap for many experiments being now performed on the nanoscale but also as a rich dataset from which theoretical models can be developed and refined. It also represents my modest contribution to the great puzzle of geometrical organization of Nature, perhaps even substantiating the daunting thesis that the complex order present in living matter comes largely as a consequence of physical constraints[7]. In a sense, this work represents just one of many facets of harnessing geometry for target pattern design.

References for Chapter 1

(1)   Plato. *Timaeus*; 360BC.
(2)   Kepler, J. *Mysterium Cosmographicum*; 1596.
(3)   Cromwell, P. R. *Polyhedra*; Cambridge University Press, 1999.
(4)   Paulsen, C. E.; Armache, J.-P.; Gao, Y.; Cheng, Y.; Julius, D. Structure of the TRPA1 Ion Channel Suggests Regulatory Mechanisms. *Nature* **2015**, *520*, 511–517.
(5)   Pauling, L. The Architecture of Molecules. *Proc. Natl. Acad.* **1964**, *51*, 977.
(6)   Bragg, W. H.; Bragg, W. L. The Structure of the Diamond. *Proc. R. Soc. London* **1913**, 277–291.
(7)   Thompson, D. *On Growth and Form.*; Cambridge Univ. Press, 1942.

Chapter 2

Models and Methods

Simulations. The simulations performed in this work were typical isochoric (constant volume) and isobaric (constant pressure) hard particle Monte Carlo simulations[1] with the use of a more sophisticated polyhedra overlap determination based on the Gilbert-Johnson-Keerthi algorithm[2]. Update steps consist of arbitrary translation, rotation and box shearing moves. Step sizes are chosen to achieve an average acceptance probability of 30%, following Frenkel and Smit[1]. While the simulation box is in principle allowed to have arbitrary dimensions and to undergo shear in any of three orthogonal directions, we use a lattice reduction technique[3] after each box move to keep the box as compact as possible and avoid strong shearing. For each polyhedron, an initial set of 12 simulations with 2048 polyhedra was run at packing fractions 49% ≤ ϕ ≤ 60% for $3 \cdot 10^7$ MC cycles. Most polyhedra assembled under these conditions. If self-assembly was not successful, then we ran longer simulations of 10^8 MC cycles and packing fractions up to 63%. If still no crystallization was observed, the system was labeled "disordered". For the complex topologically close-packed phases, larger systems of up to 10000 particles were studied to determine the crystal structure unambiguously. While cubic boxes were chosen for the assembly figures for aesthetic purposes, all systems were studied with variable box shapes. All those functionalities can be found in Michael Engel's Monte Carlo incsim[4] code, which was used throughout this work.

Geometric representation. The position and orientation of a polyhedron are given by a translation vector (x, y, z) and a quaternion (a, b, c, d). The relation between the

quaternion and the rotation matrix is:

$$R = \begin{pmatrix} a^2 + b^2 - c^2 - d^2 & 2(bc - ad) & 2(bd + ac) \\ 2(bc + ad) & a^2 - b^2 + c^2 - d^2 & 2(cd - ab) \\ 2(bd - ac) & 2(cd + ab) & a^2 - b^2 - c^2 + d^2 \end{pmatrix}.$$

Densest packings calculations. Candidates for putative densest packings are obtained by compressing systems with 1, 2, or 4 particles in the box applying periodic boundary conditions. Lattice reduction (used to keep the box as compact as possible and avoid strong shearing) is employed and, differently from the self-assembly simulations, the possibility of a particle overlapping with its own image is also considered. The protocol for densest packing calculations is as follows: for each shape, several systems (typically 50) initialized with different random seeds are independently simulated. For each of those copies, the pressure is exponentially increased according to the formula $P^* = 10^{0.01*i}$, where $i = 20, 21,$ … 700, which guarantees that the system starts reasonably dilute ($P_0 = 1.58$) and gets exponentially denser until $P_F = 10^7$ is achieved. For all the simulations referred to in this work, this protocol was enough for the putative densest packings to be achieved in a large fraction of the simulations performed. For more complex shapes, where a large majority of the simulations were not achieving the densest packing previously recorded, a different protocol was employed: in this protocol, for each pressure, multiple (typically 50) simulations were independently performed and the configuration with densest packings, at this pressure, was used for the next pressure increment. By doing so, simulations of complex, chiral shapes were found to pack denser than what was found via the first protocol but, still, only a fraction of simulations achieve the densest known packing for those shapes.

Structure characterization. For the determination of radial distribution functions and the calculation of diffraction patterns *via* fast Fourier transform, point 'scatterers' are placed in the centroids of the polyhedra. Bond order diagrams are obtained by projecting the vectors connecting the centroids of nearest neighbor polyhedra on the surface of a sphere. All three functions are used to characterize and identify the self-assembled structures and densest packings.

Analysis of local and global order. We define *nearest neighbors* as pairs of polyhedra corresponding to the first peak of the radial distribution function calculated from the

centroids. The *coordination number* (CN) is the number of nearest neighbors and is calculated by integrating the time-averaged radial distribution function from zero to the first local minimum. In the same sense, *Voronoi cells* are calculated using centroids. Fourier transforming the centroids generates *diffraction patterns*. *Bonds* connect nearest neighbors. Given polyhedra with centroids r_j and rotation matrices M_j, the *bond order diagram* is the distribution of bonds $\{r_j - r_i, i$ bonded to $j\}$ projected on the surface of the unit sphere. Analogue to the bond order diagram, we define the *orientational correlation diagram* as the distributions of vectors $\{M_j M_i^{-1}(r_j - r_i), i$ bonded to $j\}$ on the surface of a sphere. The orientational correlation diagram is sensitive to the rotation of pairs of neighbors around the bond connecting their centroids.

Crystal structure determination. To identify a crystal structure, atoms are positioned at the centroids of polyhedra. We consider this replacement when we say that an arrangement of polyhedra is isostructural to an atomic crystal. In a first step, crystal structures were analyzed in real space using particle positions and bond-order diagrams. This allows determining whether a system is ordered or disordered. We distinguish plastic (rotator) crystals from non-rotator crystals by the absence of long-range correlations in the particle-bond and particle-particle correlation diagram. Liquid crystals are identified by the absence of Bragg peaks in the diffraction pattern along at least one spatial direction. In the case of topologically close-packed phases, the crystal structure is too complicated to analyze in real space and we compare diffraction patterns of simulation results with those of ideal crystal lattices. While the structures reported are observed reproducibly and robustly in simulation and thus expected in experiments of analogous particles, their thermodynamic stability or metastability can only be rigorously ascertained through free energy calculations, which are computationally expensive for even a single shape requiring many reference configurations, and were not performed in this work.

Characterization of polyhedra shape. In the diagrams showing the *distribution of face normal vectors*, Gaussians with fixed width and intensity proportional to the area of a polyhedron face are positioned in the direction of all face normal vectors. The *isoperimetric quotient* Q of a polyhedron P with volume V and surface area S is the scalar defined as $Q = 36\pi V^2/S^3$. The *radial shape profile* $s(r)$ is the fraction of a sphere surface that is contained inside the polyhedron, $s(r) = (4\pi)^{-1} \oiint \chi_P(r, \theta, \phi) \sin\theta \, d\theta d\phi$, where χ_P

is the characteristic function of the polyhedron with origin at the centroid. The shape profile lies between 0 and 1, and has the property $V = \int_0^\infty 4\pi r^2\, s(r)\, dr$.

Visualization. Simulation snapshots are rendered using Phong shading and ambient occlusion to improve depth perception. Functions defined on the surface of a sphere (bond order diagram, correlation diagrams) are shown in either stereographic projection (angle preserving, circular plots) or using the Mollweide projection (area preserving, elliptical plots). These functions and the diffraction patterns are temporally averaged over short simulation times to remove speckle patterns. All those visualization tools can be found at Michael Engel's Interactive Java Visualizer code (injavis)[5], which was used throughout this work. An online, interactive visualization that exemplifies many of the techniques presented here can be found at the supplementary information of Engel *et al*[6].

References for Chapter 2

(1)   Frenkel, D.; Smit, B. *Understanding Molecular Simulation: From Algorithms to Applications*; Academic press, 2001; Vol. 1.

(2)   Gilbert, E. G.; Johnson, D. W.; Keerthi, S. S. A Fast Procedure for Computing the Distance between Complex Objects in Three-Dimensional Space. *IEEE J. Robot. Autom.* **1988**, *4*, 193–203.

(3)   Lattice Reduction http://en.wikipedia.org/wiki/Lattice_reduction.

(4)   Engel, M. Incsim, 2012. Currently available at https://bitbucket.org/glotzer/incsim

(5)   Engel, M. Interactive Java Visualization (INJAVIS), 2012. Currently available at https://bitbucket.org/glotzer/injavis

(6)   Engel, M.; Damasceno, P. F.; Phillips, C. L.; Glotzer, S. C. Computational Discovery of a One-Component Icosahedral Quasicrystal via Self-Assembly. *Nat. Mater.*

Chapter 3
Directional Entropic Forces[§]

Nobody knows what entropy really is, so in a debate you will always have the advantage
Von Neumann
(on why Shannon should call his "uncertainty measure" entropy)

Entropic forces are effective forces that result from a system's statistical tendency to increase its entropy. They differ from traditional, conservative ones like van der Waals or Coulomb forces that arise from underlying microscopic interactions. Polymer "elasticity",[1] hydrophobicity[2] and depletion interactions[3] are all examples of entropic forces. Entropy can also cause hard particles, which have no interactions other than their inability to occupy the same region in space, to form crystals and liquid crystals. Hard rods and disks spontaneously align and can order into layers and columns at intermediate packing densities, if those structures increase the configurational space available to the particles.[4,5] Hard spheres crystallize into a face-centered cubic (fcc) structure for the same reason.[6] Recently, the first hard-particle quasicrystal – a complex structure with long-range order but no periodicity, mostly observed in atomic alloys – was discovered in computer simulations of regular tetrahedra.[7] Beyond simple crystals and liquid crystalline phases, experimental realizations of complex colloidal crystals, such as those isostructural to AB_n atomic crystals, have required two-component mixtures or attractive interactions,[8-10] regardless of building block shape. Finding new and alternative ways to assemble novel superstructures is an important prerequisite for future applications of nanoparticles and colloids.

[§] This chapter was originally published as "Damasceno, P. F.; Engel, M.; Glotzer, S. C. Crystalline Assemblies and Densest Packings of a Family of Truncated Tetrahedra and the Role of Directional Entropic Forces. *ACS Nano* **2011**, *6*, 23."

In this work we investigate the influence of shape on particle self-assembly and show that small changes in shape of hard polyhedra can suffice to produce a range of colloidal crystal structures whose rich complexity rivals that of atomic analogues, without the need for mixtures or attractive interactions. To demonstrate this, we study *via* computer simulation assemblies and packings of hard tetrahedra as their corners are increasingly and symmetrically truncated until the particles become octahedra. In addition to body-centered cubic and quasicrystalline structures, we report a space-filling polyhedron forming b-tin, a densest packing for the Archimedean truncated tetrahedron into a-arsenic, and the self-assembly of crystals isostructural to diamond and high-pressure lithium. We show that in all cases the assembled structures favor face-to-face alignment, and, building on earlier concepts of entropy-driven phase transitions,[4,5] we introduce the notion of directional entropic forces for hard particles in analogy with controlled entropic forces in systems of colloids and with directional enthalpic forces in molecular and patchy particle systems. This notion explains the observed crystal superlattices in a natural way.

Our choice of building blocks is motivated by recent advances in the synthesis and assembly of faceted and monodisperse nanocrystals,[11-17] and especially tetrahedra.[18, 19] The observation that the structure of many atomic crystals is dominated by polyhedral building blocks[20] suggests the possibility to reproduce atomic crystal isostructures with colloidal polyhedra. However, the phase behavior of polyhedra is often unknown even for the highly symmetric Platonic and Archimedean solids. Exceptions are mesophases[21] and phases in the limit of high pressure, which are identical to maximally dense packings and have been studied as a mathematical optimization problem.[22-26] To date, no large-scale assembly simulations of complex crystal structures with thousands of polyhedra have been reported in the literature.

We use Monte Carlo computer simulation as in Ref. 7. To identify a crystal structure, each polyhedron is replaced by an atom positioned at its centroid. We consider this replacement when we say that an arrangement of polyhedra is "isostructural" to an atomic crystal. The amount of truncation applied to a tetrahedron is specified by the truncation parameter t. This parameter increases linearly with the distance of a truncation plane from the nearest of the four vertices in the original regular tetrahedron. A truncated tetrahedron has four equilateral triangles with edge length $s(t/2)$ and four hexagons with

the two edge lengths $s(1 − t)$ and $s(t/2)$. Special cases depicted in Fig. 1. 1a are the regular tetrahedron, with $t = 0$, the (as we will see) space-filling truncated tetrahedron (STT), with $t = 1/2$, the Archimedean truncated tetrahedron (ATT), with $t = 2/3$, and the regular octahedron, with $t = 1$.

Results and Discussion.

Densest packings. We first investigate the densest packings as a function of truncation. The findings are later compared to the self-assembled structures. Results for the maximum packing density f_{max} are included in Figs. 1b and 2a. We find that $f_{max}(t)$ is continuous, but shows sharp kinks.[26] The observation that all truncated tetrahedra pack with densities of at least $f_{max} = 82\%$ indicates that these shapes are generally efficient packers. They pack much better than spheres, which have a maximum packing density of only 74%. The number of particles per primitive unit cell jumps from $n = 4$ for weakly truncated tetrahedra ($t < 0.27$), to $n = 2$ for intermediate cases ($0.27 < t < 0.93$), and finally to $n = 1$ for strongly truncated tetrahedra resembling octahedra ($t > 0.93$). This decrease in n is expected because shapes tend to pack into simpler configurations with fewer particles per unit cell if they are more centrally symmetric.[24] We observe that neighboring particles always pack face-to-face with at least partial registry. For $n = 2$, the orientations of the two truncated tetrahedra are related by inversion. For $n = 4$, the particles form two dimers which are again related by inversion.

A further classification is possible by studying the geometry of the primitive unit cell with varying t. We observe that the unit cell of the densest packing shears smoothly with t when contact points between neighbors can be maintained and slide along the particle surfaces. A kink in $f_{max}(t)$ appears if there is a denser packing with a different neighbor configuration, or if a contact point hits an edge of a polyhedron as t changes, in which case deformations require the unit cell to shear in another direction. The lattice parameters of the densest packings are shown in Fig. 1. 2b. The variation of the lattice parameters with truncation exhibits several transitions. Symmetric packings (monoclinic, tetragonal, orthorhombic) occur for intermediate truncations. Shapes close to the octahedron favor triclinic lattices. As reported previously, perfect tetrahedra arrange as dimers and pack most densely in a triclinic double dimer packing[25,26] and octahedra pack

most densely in a rhombohedral Bravais lattice.[22]

New packings appear for $t = 1/2$ and $t = 2/3$, both local maxima of $f_{max}(t)$ in Fig. 1. 1b. The STT at $t = 1/2$ (Fig. 1. 2d) has $f_{max}(t) = 1$ and is therefore space filling. The centroids of the STT form the b-tin structure (Supplementary Information, Fig. 1. S1). The exact analytical positions and orientations of the STT in this structure are given in Table S1. It appears the STT tiling has been missed in previous searches[27] and thus the STT is a previously unrecognized space-filling polyhedron. Given the simplicity and high symmetry of the STT and the sparsity of space-filling polyhedra in general, this discovery is unexpected.

The importance of the packing at $t = 2/3$ lies in the regularity of the ATT. As an Archimedean solid, the ATT has four regular hexagonal faces and four regular triangular faces. Based on the findings in our simulations, we analytically construct an ideal tiling of ATT with packing density $f_{max} = 207/208$ (Fig. 1. 2e). A similar packing density has also recently been reported[28] in parallel to this work. Other previous studies have reported packings with densities $f_{max} = 23/24$ [24] and $f_{max} = 0.988...$[29] for the ATT. Although the number of the densest ATT packing is surprisingly close to 1, the ATT does not fill space because of the appearance of small tetrahedral voids with edge length $s/9$. The centroids of the ATT form the a-arsenic structure (Fig. 1. S2). The exact analytic construction of the ATT packing is given in Table S2.

Self-assembly of crystal structures. Next we study the self-assembly of hard truncated tetrahedra into crystals starting from the disordered fluid phase. We choose a truncation t and an initial packing density f for a constant volume Monte Carlo simulation and simulate for 20-100 million of Monte Carlo cycles. The lowest packing density where we observe crystallization, f_c, is shown as the lower curve in Fig. 1. 1b. Crystallization does not occur on the timescale of our simulations in the region $0.8 < t < 0.85$, indicating that either the nucleation rate is extremely low, or crystals are not possible. For all other ranges of t between 0 and 1, we repeatedly observe nucleation and rapid growth of single-crystal phases spanning the whole simulation box. We find that f_c varies between 0.5 and 0.63 depending on shape and increases towards the boundaries of the stability regimes.

Five crystal structures spontaneously self-assemble in our simulations as t is increased from zero. Over a considerable range of truncation ($0 \leq t \leq 0.45$), the particles

order into a dodecagonal quasicrystal (Fig. 1. 3a). This shows that the quasicrystal reported previously with regular tetrahedra[7] is robust and forms even with truncated particles. However, as t increases towards 0.5, crystallization slows and the quality of the quasicrystal deteriorates. For $0.5 \leq t \leq 0.8$, the diamond structure assembles from the fluid. Nucleation is fast and crystal growth is robust enough to obtain defect-free single crystals routinely with thousands of particles (Fig. 1. 3b). Towards the higher end of this range of t, the cubic unit cell of diamond compresses along one direction to form the tetragonal crystal structure b-tin, identical to the densest packing of the STT, but for different values of t.

Strongly truncated tetrahedra with $0.85 \leq t < 0.95$ assemble into a cubic phase isostructural to high-pressure lithium.[30] The lattice is bipartite and comprised of two identical but intertwined sublattices, as indicated by the coloring in Fig. 1. 3c. Although the structure is complex with 16 particles in the unit cell, perfect single crystals assemble easily from the fluid (Fig. 1. S5). To our knowledge, crystals with such a high number of particles in the unit cell have so far not been reported for hard particles in the literature. For nearly perfect octahedra ($0.95 \leq t \leq 1$), the body-centered cubic (bcc) lattice is observed at low density (Fig. 1. 3d). This is expected because nano-octahedra with short-range repulsive interactions self-assemble into bcc.[31]

It is interesting to note that the densest packing is different from the stable phase nucleating from the fluid (Fig. 1. 1b). We do not find even one value for the truncation parameter t, where the densest packings and assembled crystals are identical. Even in the case of perfect octahedra, the bcc crystal at low density transforms into a rhombohedral lattice by a slight shear along the [111] direction. This indicates that the self-assembly of hard truncated tetrahedra, and possibly of a large class of polyhedra, cannot be viewed as a packing problem alone. We further observe that the self-assembled structures typically have higher crystallographic symmetry (tetragonal, cubic, dodecahedral) compared to their corresponding densest packings (triclinic, monoclinic, tetragonal, orthorhombic) and have more face-to-face orientations between nearest neighbors.

Directional entropy. Indeed, face-to-face arrangements appear to be a key motif in the self-assembly of hard polyhedra. The crystals we observe can be grouped into three classes with varying symmetries and varying importance of face-to-face orientations: (i)

bcc-like structures, (ii) a tetrahedral network, and (iii) carbon-related structures. The bcc-like structures (bcc, high-pressure lithium) result for particles with shapes resembling the octahedron. The high-pressure lithium phase relates closely to bcc by shifting atom columns.[30] Within each sublattice of the bipartite lithium structure there are hexagon-hexagon face-to-face contacts only (Fig. 1. 3c), while triangle-hexagon and triangle-triangle orientations occur only between sublattices (Fig. 1. S4). It is interesting that the high-pressure lithium phase has recently also been observed with attractive octahedral nanocrystals,[32] which demonstrates that in this example changing the shape of the octahedron to a truncated tetrahedron has a similar effect on the preferred crystal structure as turning on an attractive face-to-face interaction. In bcc, the higher equivalence of triangle and hexagon faces facilitates two types of face-to-face orientations (Fig. 1. S6), explaining the transition from high-pressure Lithium to bcc for increasing values of the truncation parameter.

At the other extreme, the dodecagonal quasicrystal can be understood as a tetrahedral network of pentagonal dipyramids.[7] It occurs for particles with shape most closely resembling the tetrahedron and is dominated by triangular face-to-face contacts that produce dimers arranged in stacks of pentagonal dipyramids and 12-member rings. Shapes intermediate between the tetrahedron and the octahedron form a range of carbon-like structures, including diamond, b-tin, and a-arsenic, with strong face-to-face alignment of hexagonal facets. In contrast to the tetrahedral network, neighboring faces are now rotated by 180 degrees relative to each other, which permits a higher contact area for these truncations (Fig. 1. S3).

Thermodynamic systems minimize free energy at equilibrium; when interactions are absent, entropy is maximized at fixed volume. The favoring of face-to-face orientations provides insight into how entropy is maximized by the structures we observe. Consider the well-known, isotropic-to-nematic transition in hard rods.[4] At sufficiently high packing densities, parallel alignment increases the translational entropy of the system at the expense of rotational entropy, producing the nematic phase.[5] Simple analogy suggests that polyhedra should likewise prefer to align with faces parallel, in agreement with our observations. Competition among different types of faces, as in the present family of polyhedra, can lead to complexity of structure.

Conclusion. Our simulation results constitute the first report of the self-assembly of complex crystal structures from the fluid phase with hard particles. The findings can be explained by a preference for face-to-face alignment in systems of hard, faceted objects, which suggests considering entropic forces as directional in such systems, since they increase with contact area between neighbors[3] and thus act strongest perpendicular to the faces. In this sense, directional entropic forces in hard particle systems act like attractive interactions in systems of patchy particles, or like depletion interactions in mixtures of large and small particles, which can be controlled by shape [17, 33] and roughness.[34] Our results suggest that particle shape can produce entropic "patchiness" just as patterning can produce interaction patchiness[35] and that bond geometries in patchy particle systems can, in principle, be imitated by shape, providing additional strategies for building block design. A recent example of directional entropic forces in colloids are dimpled "pacman" particles,[33] in which the dimple shape and entropic depletion forces control particle binding. The use of depletants with polyhedral particles should provide an even greater variety of ordered structures, obtained then by entropic patchiness arising both from facet alignment and anisotropic depletion.
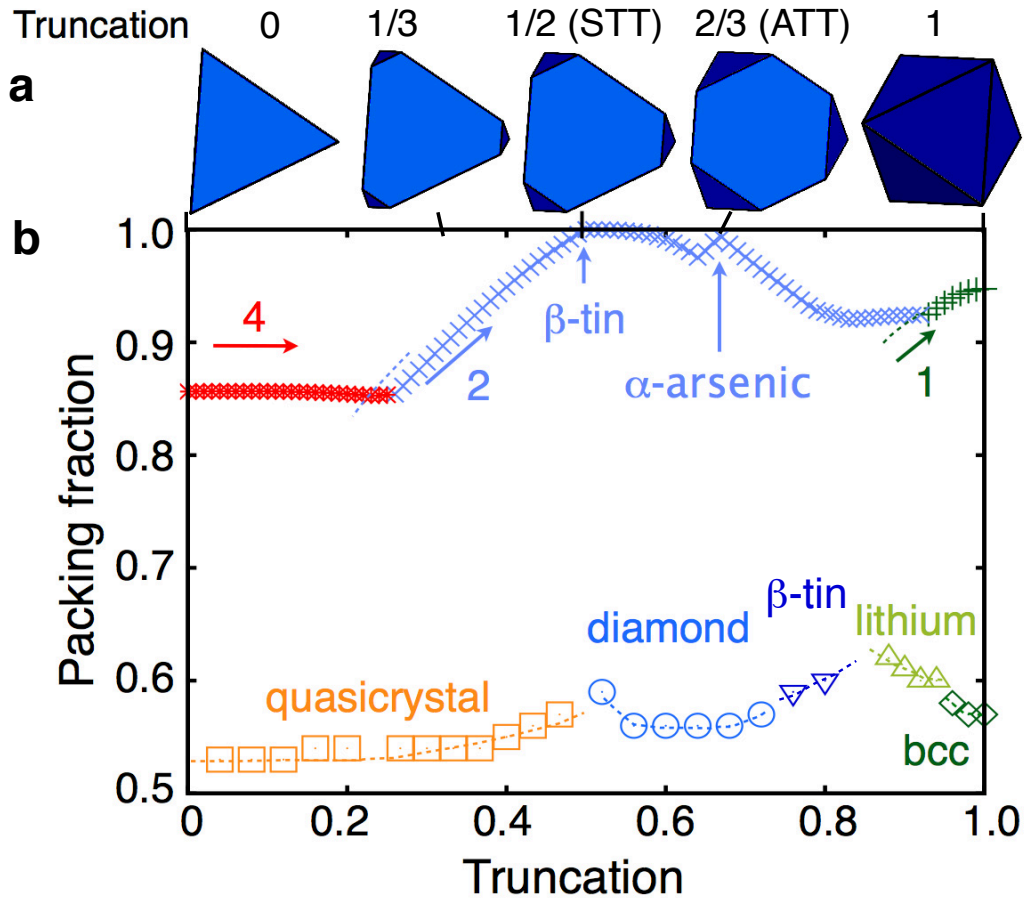
Figure 3.1. Dense packings and self-assembled truncated tetrahedra into atomic crystal isostructures. a, The family of truncated tetrahedra is parameterized by the truncation parameter *t* and ranges from the regular tetrahedron to the regular octahedron. **b,** Phase diagram of truncated tetrahedra. Upper datasets indicate maximum packing densities f_{max}. Numerals and corresponding colors indicate the number of particles in the primitive unit cell. Labels indicate b-tin and a-arsenic structures for the space-filling and Archimedean truncated tetrahedra, respectively. Lower datasets corresponds to the lowest density, f_c, at which crystallization from the fluid is observed. Labels indicate the dodecagonal quasicrystal, diamond, b-tin, high-pressure lithium, and body-centered cubic structures.
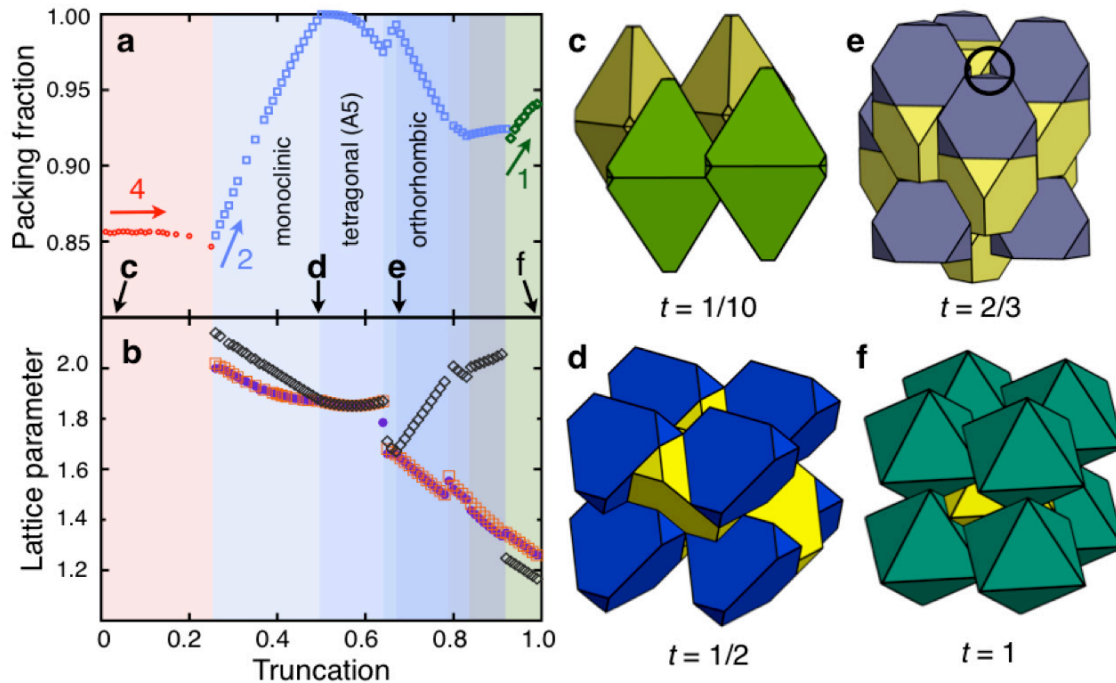
Figure 3.2. Densest packings of truncated tetrahedra. a, Blow-up of maximum packing densities from Fig. 1. 1b and comparison with **b,** lattice parameters vs. truncation t. Colors of the data sets in (a) (red, blue green) indicate the number of particles in the primitive unit cell (four, two, one) for indicated structures. Colors of the data sets in (b) (magenta, dark blue, dark green) indicate the absolute value of the three lattice parameters that generate the unit cell. In both (a) and (b), vertical background shading indicates unit cells with different numbers of particles or different symmetries (vertical regions inside blue shading). Discontinuities of the derivative of f_{max} occur at $t = 0.50$, 0.64, $2/3$, 0.78, 0.83 and 0.94, and indicate changes in symmetry of the densest packing structure. These kinks are reflected by similar discontinuities in the lattice parameter curve (or its derivative) in (b). **c,** For small truncations the particles form dimers, which occur in two orientations similar to the densest tetrahedron packing. **d,** The STT fills space in the b-tin structure. Two triangular faces fit along a long edge of the hexagonal faces. **e,** The ATT packs with a density of 207/208 in a lattice isostructural to a-arsenic. The particles are perfectly face-to-face within dimers, but not with other neighbors. **f,** Regular octahedra pack into a rhombohedral Bravais lattice, which is slightly sheared compared to the bcc lattice.

16
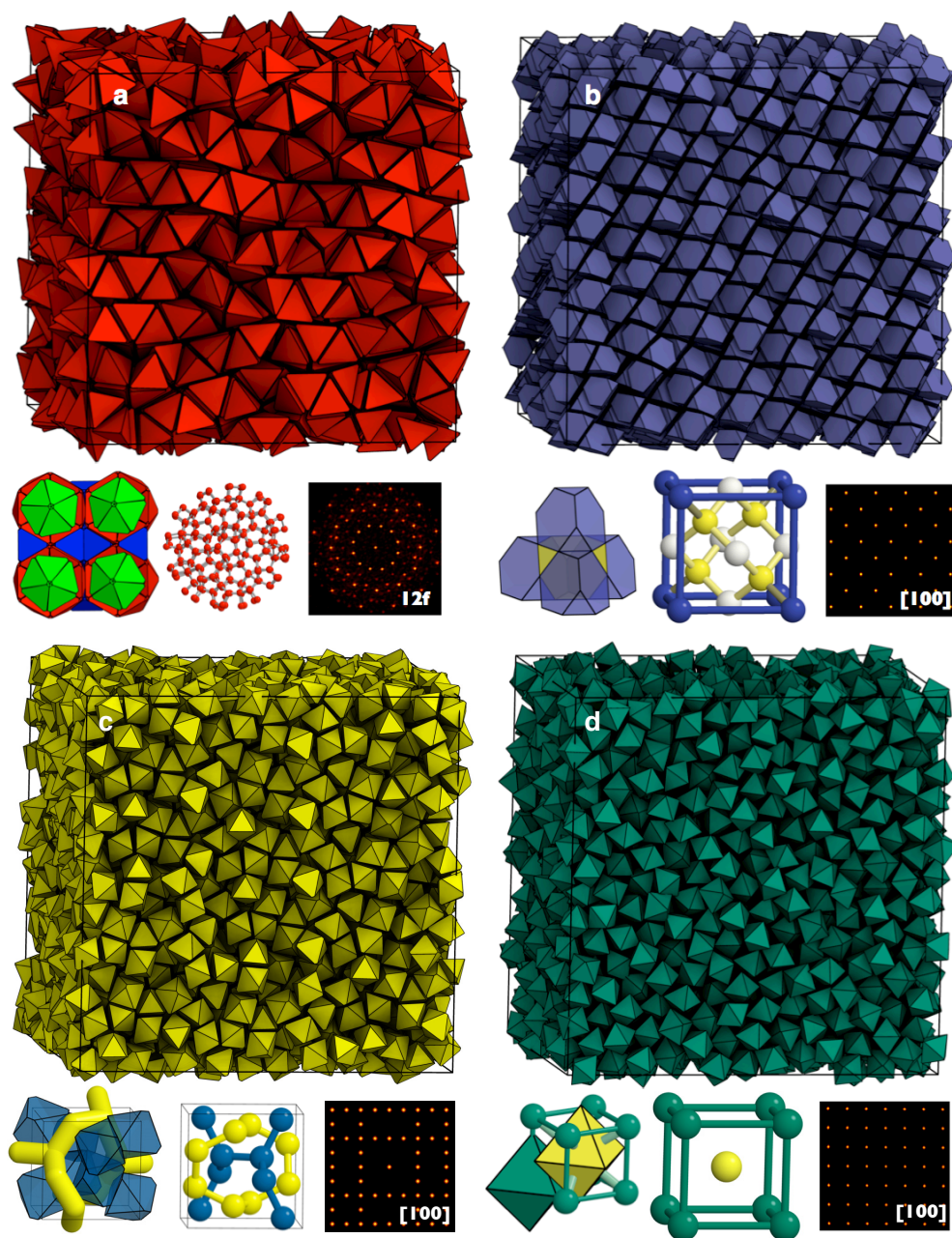
Figure 3.3. Structures of truncated tetrahedra self-assembled in simulation at intermediate density. In each subfigure a snapshot of the full simulation box, temporally averaged to remove thermal disorder together with a characteristic motif (bottom left), ball-and-stick model (bottom center) and the system's diffraction pattern (bottom right) are shown. With increasing truncation, 2624 truncated tetrahedra assemble into **a,** dodecagonal quasicrystal ($t = 0.2$), **b,** diamond lattice ($t = 2/3$), **c,** bipartite lattice isostructural to high-pressure lithium ($t = 0.95$), and **d,** bcc lattice of regular octahedra ($t = 1$). Not shown: b-tin ($t = 0.8$), which is the same structure as that obtained for the densest STT structure at a different value of t.
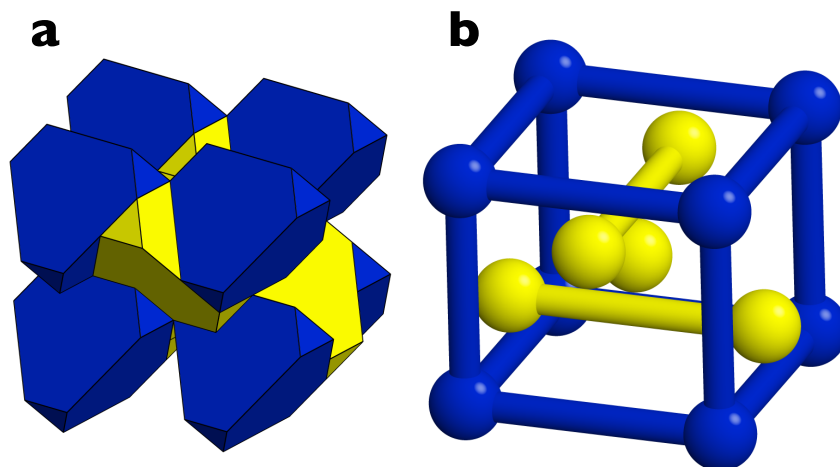
Figure 3.4. The packing of space filling truncated tetrahedra (STT). a, Snapshot of the particles arranged into the b-tin structure (Strukturbericht designation A5, tetragonal diamond) with lattice parameters of the non-primitive cell $a = 1.6^{-1/2}s$ and $c = 2.0^{-1/2}s$, and space group I4$_1$/amd (No. 141). Note that the edge lengths of the hexagonal facets have a ratio of 2:1, which allows neighboring STT to align effectively along edges. The STT tiling is intricate because neighboring polyhedra are only in partial face-to-face contact. **b,** Ball-and-stick model of b-tin.

a	Lattice Vectors	b_1 = (6, −2, −4); b_2 = (−2, −6, 4); b_3 = (−6, 2, −4)
b	Vertices of the space-filling truncated tetrahedron	v_1 = (4, 2, 2); v_2 = (2, 4, 2); v_3 = (2, 2, 4); v_4 = (4, −2, −2); v_5 = (2, −2, −4); v_6 = (2, −4, −2); v_7 = (−2, 4, −2); v_8 = (−2, 2, −4); v_9 = (−4, 2, −2); v_{10} = (−2, −2, 4); v_{11} = (−2, −4, 2); v_{12} = (−4, −2, 2)
c	Particle 1	position = (2, 1, 1); orientation = (1, 0, 0, 0)
d	Particle 2	position = (−2, −1, −1); orientation = (cos(p / 4), sin(p / 4), 0, 0)

Table 3.1. Structural data of the packing of space filling truncated tetrahedra (STT) with two particles in the unit cell. a, Lattice vectors spanning the unit cell. **b,** The twelve vertices of the STT in standard orientation positioned at the origin. **c,d,** Positions and orientations of the two particles.
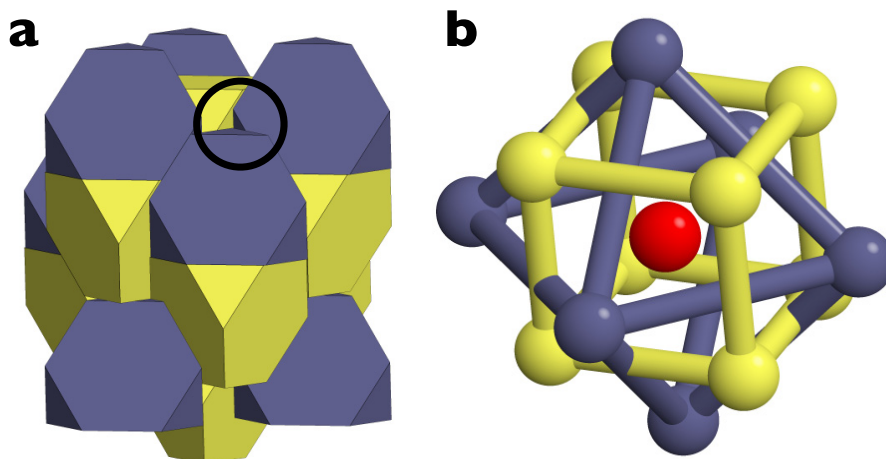
Figure 3.5. The densest packing of the Archimedean truncated tetrahedron (ATT) with packing density f_{max} = 207/208. a, Snapshot of the particles arranged into the a-arsenic structure (Strukturbericht designation A7) with three lattice parameters $a \approx 0.3984s$, $b \approx -0.1682s$, $u = 72^{-1/2}s$ and space group $R\bar{3}m$ (No. 166). The packing is not space-filling because of small tetrahedral voids found between the dimers. One such void is indicated by a black circle. **b,** Ball-and-stick model of a-arsenic.

a	**Lattice Vectors**	$b_1 = (-4, 8, 12)$; $b_2 = (12, -4, 8)$; $b_3 = (8, 12, -4)$
b	**Vertices of the Archimedean truncated tetrahedron**	$v_1 = (9, 3, 3)$; $v_2 = (3, 9, 3)$; $v_3 = (3, 3, 9)$; $v_4 = (9, -3, -3)$; $v_5 = (3, -3, -9)$; $v_6 = (3, -9, -3)$; $v_7 = (-3, 9, -3)$; $v_8 = (-3, 3, -9)$; $v_9 = (-9, 3, -3)$; $v_{10} = (-3, -3, 9)$; $v_{11} = (-3, -9, 3)$; $v_{12} = (-9, -3, 3)$
c	**Particle 1**	position = $(3, 3, 3)$; orientation = $(1, 0, 0, 0)$
d	**Particle 2**	position = $(-3, -3, -3)$; orientation = $(\cos(\pi/4), \sin(\pi/4), 0, 0)$

Table 3.2. Structural data of the packing of Archimedean truncated tetrahedra (ATT) with two particles in the unit cell. a, Lattice vectors spanning the unit cell. **b,** The twelve vertices of the ATT in standard orientation positioned at the origin. **c,d,** Positions and orientations of the two particles.
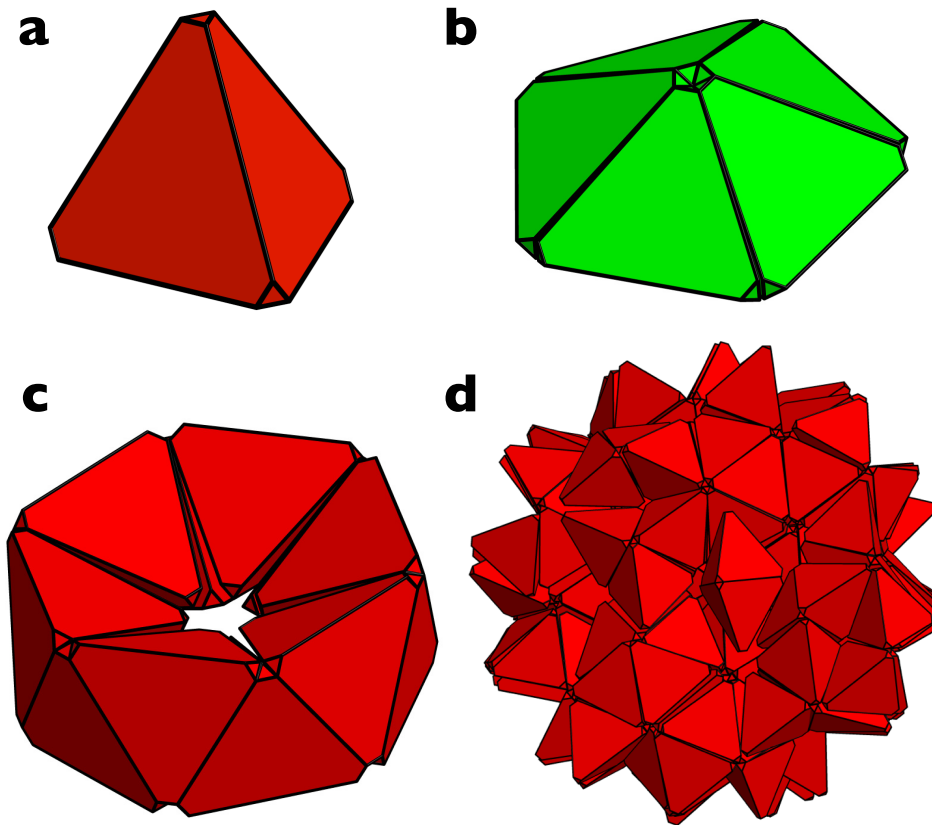
Figure 3.6. Hierarchical assembly of slightly truncated tetrahedra into a dodecagonal quasicrystalline structure. a, Slightly truncated tetrahedra ($t = 0.1$) form **b,** pentagonal dipyramids of five particles and **c,** rings consisting of twelve particles. These local building blocks ultimately assembly into a 12-fold quasicrystal. A small patch of the quasicrystal is shown in **d**.
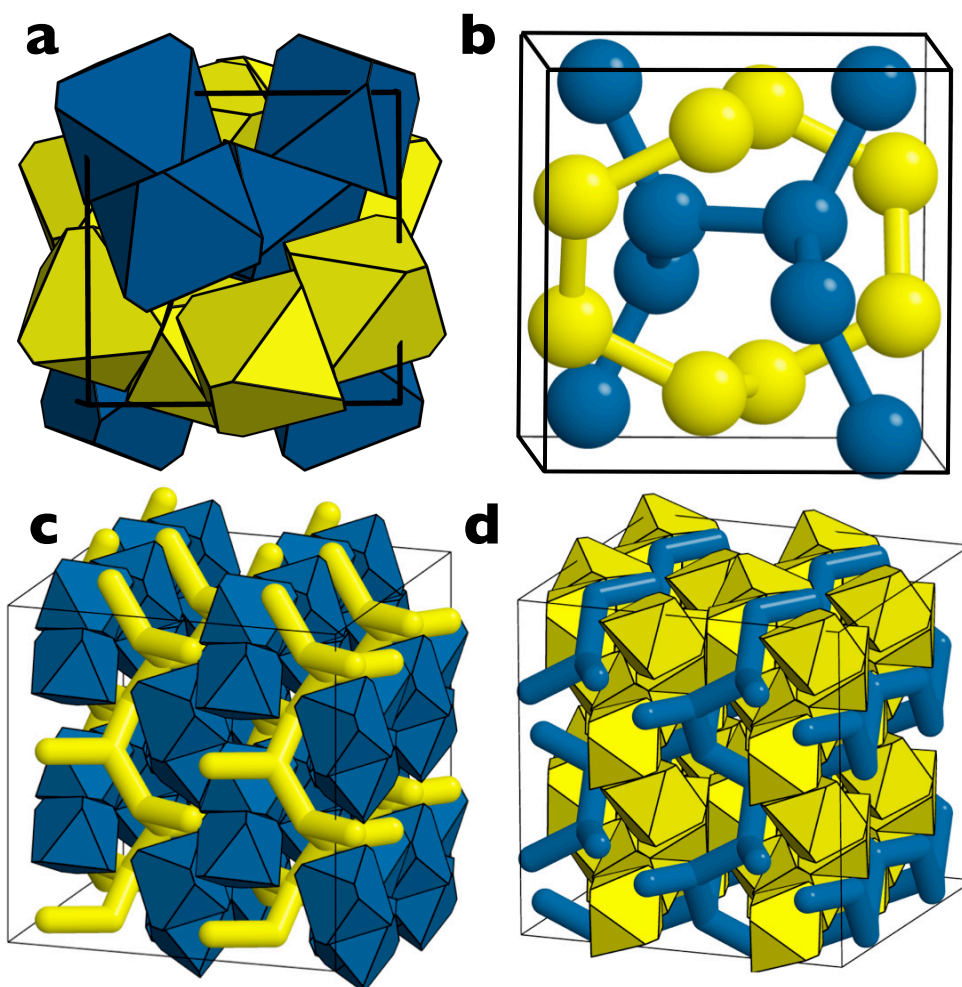
Figure 3.7. Highly truncated tetrahedra ($t = 0.9$) resembling octahedra self-assemble into a phase isostructural to high pressure lithium. a, Snapshot of the cubic unit cell. Each truncated tetrahedron is connected to three nearest neighbors along its hexagonal faces. The connection splits the structure up into two sublattices as indicated by the coloring (yellow and blue). **b,** The centroids of the nearest neighbors are connected with bonds showing the two sublattices. **c,d,** The two sublattices shown separately. The sublattices are not connected to each other via nearest neighbor bonds.
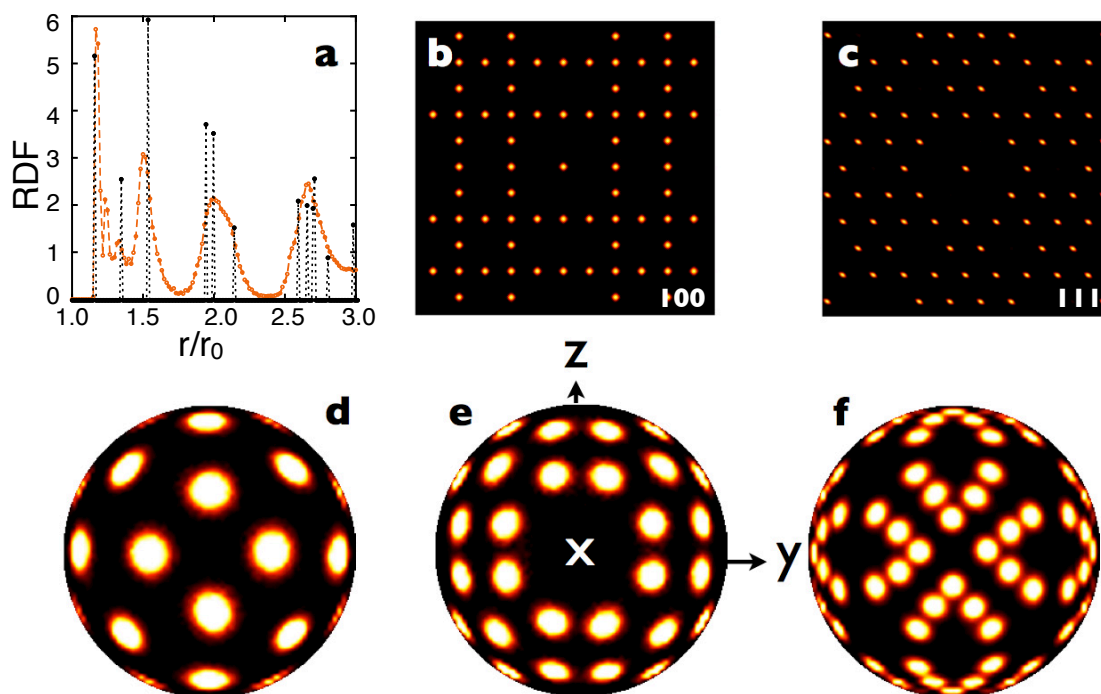
Figure 3.8. Structural characterization of the phase isostructural with high pressure lithium. a, Radial distribution function of a perfect (black) and self-assembled system (orange) composed of 2624 truncated tetrahedra. **b-c,** Diffraction pattern along [100] and [111] crystallographic directions. **d-f,** Bond order diagrams along the x-direction. The diagrams correspond to the neighbors found within a distance covered by the first peak, 1.0 < r < 1.4 (d), the second peak, 1.4 < r < 1.75 (e), and the third peak, 1.75 < r < 2.4 (f) of the radial distribution function.
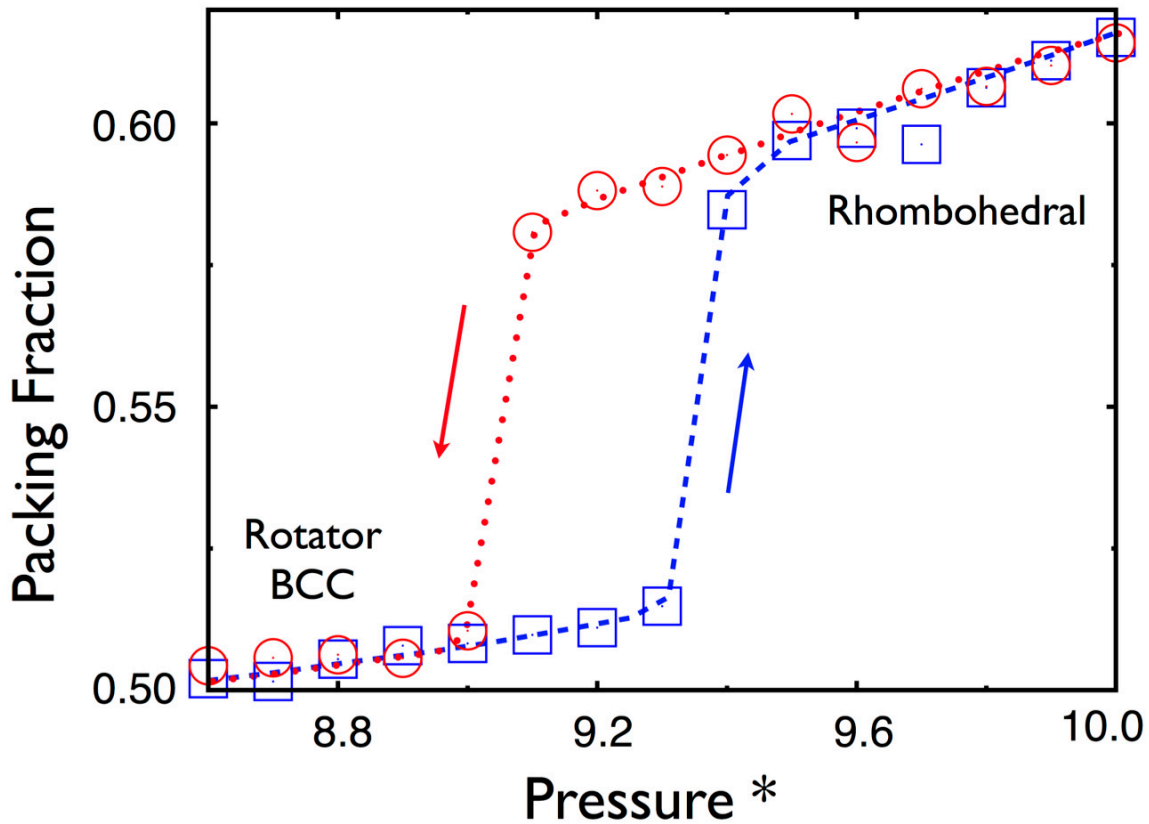
Figure 3.9. Equation of state calculated for perfect octahedra. Equation of state from simulations of perfect octahedra (t=1). The blue points represent systems of 1024 particles initially in a rotator bcc phase that undergoes a first-order phase transition to the rhombohedral phase under compression. The red line, conversely, represents systems initially in the rhombohedral packing that transform into the rotator bcc phase under decompression.
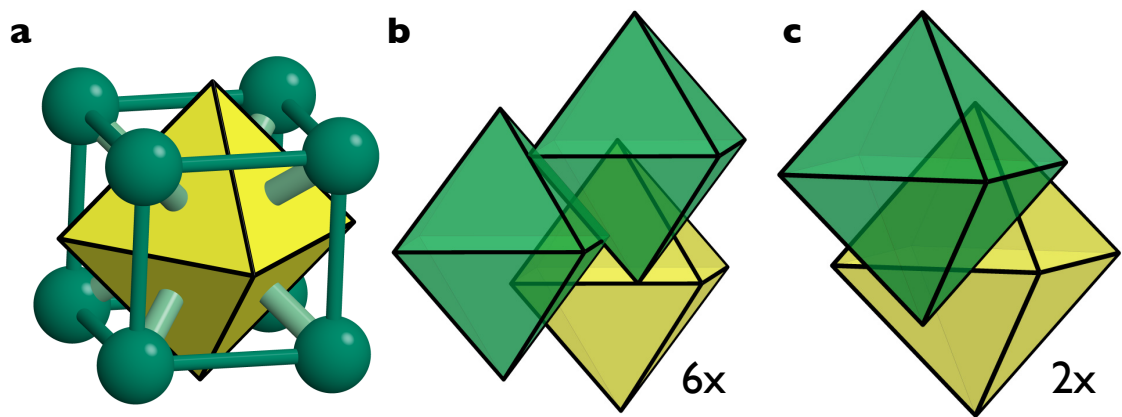
Figure 3.10. Arrangement of octahedra into a weakly sheared bcc lattice. a, The orientation of the octahedra breaks the cubic symmetry. Six of its eight faces align face-to-face with neighbors as shown in **b**. The two remaining phases align as shown in **c**.

References for Chapter 3

(1)   de Gennes, P. G. Scaling Concepts in Polymer Physics. *Cornell University Press* **1979.**

(2)   Chandler, D. Interfaces and the Driving Force of Hydrophobic Assembly. *Nature* **2005,** 437, 640-647.

(3)   Lekkerkerker, H. N. W.; Tuinier, R. Colloids and the Depletion Interaction. *Dordrecht: Springer, Netherlands* **2011.**

(4)   Onsager, L. The Effects of Shape on the Interaction of Colloidal Particles. *Annals of the New York Academy of Sciences* **1949,** 51, 627-659.

(5)   Frenkel, D. Entropy-driven Phase Transitions. *Physica A* **1999,** 263, 26-38.

(6)   Kirkwood, J. G. Crystallization as a Cooperative Phenomenon. *Phase Transformations in Solids* **1951.**

(7)   Haji-Akbari, A.; Engel, M.; Keys, A. S.; Zheng, X.; Petschek, R. G.; Palffy-Muhoray, P.; Glotzer, S. C. Disordered, Quasicrystalline and Crystalline Phases of Densely Packed Tetrahedra. *Nature* **2009,** 462, 773-777.

(8)   Leunissen, M. E.; Christova, C. G.; Hynninen, A. P.; Royall, C. P.; Campbell, A. I.; Imhof, A.; Dijkstra, M.; van Roij, R.; van Blaaderen, A. Ionic Colloidal Crystals of Oppositely Charged Particles. *Nature* **2005,** 437, 235-240.

(9)   Shevchenko, E. V.; Talapin, D. V.; Kotov, N. A.; O'Brien, S.; Murray, C. B. Structural Diversity in Binary Nanoparticle Superlattices. *Nature* **2006,** 439, 55-59.

(10)   Kalsin, A. M.; Fialkowski, M.; Paszewski, M.; Smoukov, S. K.; Bishop, K. J.; Grzybowski, B. A. Electrostatic Self-assembly of Binary Nanoparticle Crystals with a Diamond-like Lattice. *Science* **2006,** 312, 420-424.

(11)   Glotzer, S. C.; Solomon, M. J. Anisotropy of Building Blocks and their Assembly into Complex Structures. *Nature materials* **2007,** 6, 557-562.

(12)   Li, F.; Josephson, D. P.; Stein, A. Colloidal Assembly: the Road from Particles to Colloidal Molecules and Crystals. *Angew Chem Int Ed Engl* **2011,** 50, 360-388.

(13)   Tian, N.; Zhou, Z. Y.; Sun, S. G.; Ding, Y.; Wang, Z. L. Synthesis of Tetrahexahedral Platinum Nanocrystals with High-index Facets and High Electro-oxidation Activity. *Science* **2007,** 316, 732-735.

(14)   Quan, Z.; Fang, J. Superlattices With Non-spherical Building Blocks. *Nano Today* **2010,** 5, 390-411.

(15)   Lu, F.; Lelie, D.; Gang, O. Continuous Phase Transformation in Nanocube Assemblies. *Physical Review Letters* **2011,** 107, 135701.

(16)   Personick, M. L.; Langille, M. R.; Zhang, J.; Mirkin, C. A. Shape Control of Gold Nanoparticles by Silver Underpotential Deposition. *Nano Lett* **2011,** 11, 3394-3398.

(17)   Zhao, K.; Bruinsma, R.; Mason, T. G. Entropic Crystal-crystal Transitions of Brownian Squares. *Proc Natl Acad Sci U S A* **2011,** 108, 2684-2687.

(18)   Chiu, C. Y.; Li, Y.; Ruan, L.; Ye, X.; Murray, C. B.; Huang, Y. Platinum Nanocrystals Selectively Shaped Using Facet-specific Peptide Sequences. *Nat Chem* **2011,** 3, 393-399.

(19)   Srivastava, S.; Santos, A.; Critchley, K.; Kim, K. S.; Podsiadlo, P.; Sun, K.; Lee, J.; Xu, C.; Lilly, G. D.; Glotzer, S. C.; et al. Light-controlled Self-assembly of Semiconductor Nanoparticles into Twisted Ribbons. *Science* **2010,** 327, 1355-1359.

(20)   Lord, E. A.; Mackay, A. L.; Ranganathan, S. New Geometries for New Materials. *Cambridge University Press* **2006.**

(21) Agarwal, U.; Escobedo, F. A. Mesophase Behaviour of Polyhedral Particles. *Nat Mater* **2011,** 10, 230-235.

(22) Minkowski, H. Dichteste gitterförmige Lagerung kongruenter Körper. *Nachr. Ges. Wiss. Göttingen* **1904,** 311-355.

(23) Betke, U.; Henk, M. Densest Lattice Packings of 3-polytopes. *Computational Geometry* **2000,** 16, 157-186.

(24) Torquato, S.; Jiao, Y. Dense Packings of the Platonic and Archimedean Solids. *Nature* **2009,** 460, 876-879.

(25) Chen, E. R.; Engel, M.; Glotzer, S. C. Dense Crystalline Dimer Packings of Regular Tetrahedra. *Discrete Comput Geom* **2010,** 44, 253-280.

(26) Kallus, Y.; Elser, V. Dense-packing Crystal Structures of Physical Tetrahedra. *Physical Review E* **2011,** 83, 036703.

(27) Goldberg, M. On the Space-filling Octahedra. *Geometriae Dedicata* **1981,** 10, 323-335.

(28) Jiao, Y.; Torquato, S. Communication: A Packing of Truncated Tetrahedra that Nearly Fills all of Space and its Melting Properties. *The Journal of Chemical Physics* **2011,** 135, 151101.

(29) de Graaf, J.; Rene, v. R.; Dijkstra, M. Dense Regular Packings of Irregular Nonconvex Particles. *Physical Review Letters* **2011,** 107, 155501.

(30) Hanfland, M.; Syassen, K.; Christensen, N. E.; Novikov, D. L. New High-pressure Phases of Lithium. *Nature* **2000,** 408, 174-178.

(31) Zhang J.; Luo Z.; Quan Z.; Wang Y.; Kumbhar A.; Smilgies D-M.; Jiye F. Low Packing Density Self-Assembled Superstructure of Octahedral Pt3Ni Nanocrystals. *Nano Letters* **2011,** *11,* 2912-2918.

(32) Henzie, J.; Gruenwald, M.; A. Widmer-Cooper, Geissler, P. L.; Yang, P. Self-assembly of Uniform Polyhedral Silver Nanocrystals into Densest Packings and Exotic Superlattices. *Nature Materials* **2011** in press

(33) Sacanna, S.; Irvine, W. T.; Chaikin, P. M.; Pine, D. J. Lock and Key Colloids. *Nature* **2010,** 464, 575-578.

(34) Zhao, K.; Mason, T. G. Directing Colloidal Self-assembly Through Roughness-controlled Depletion Attractions. *Phys Rev Lett* **2007,** 99, 268301.

(35) Zhang, Glotzer, S. C. Self-Assembly of Patchy Particles. *Nano Lett.* **2004,** 4, 1407-1413.

Chapter 4

A Polyhedra Zoo[**]

> *The structures of many crystals and molecules can be conveniently*
> *described by reference to the five regular polyhedra.*
> **Linus Pauling**

The spontaneous organization of individual building blocks into ordered structures is ubiquitous in Nature and found at all length scales. Examples include simple and complex crystals in atomic systems, liquid and plastic crystals in molecular materials, and superlattices of nanoparticles and colloids. Understanding the relationship between building blocks and their assemblies is essential for materials design because physical properties depend intimately on structure. The formation of atomic materials structures can be rationalized, to first approximation, from geometry considerations [1] and with growing length scale the shape of the building blocks becomes increasingly important. For colloidal particles interacting through the excluded volume arising from their shape [2–5], thermodynamic equilibrium structures ("phases") reported were relatively simple [6–10]. The simulation prediction of a dodecagonal quasicrystal with tetrahedra [11] demonstrated the unexpected complexity that could be achieved for particles solely with hard interactions. Since then, ordered structures have been reported for various polyhedra [11–16], which are now routinely synthesized as nanocrystals [4,5,13,17]. However, the a priori prediction of structure from particle shape has yet to be demonstrated.

The thermodynamic behavior of hard particles can be understood through entropy maximization [18]. Packing efficiency plays an increasingly important role towards higher

---

[**] This chapter was originally published as "Damasceno, P. F.; Engel, M.; Glotzer, S. C. Predictive Self-Assembly of Polyhedra into Complex Structures. *Science* **2012**, *337*, 453–457."

density and induces a preferential alignment of flat facets [13,19,20]. Since packing efficiency increases with contact area, the alignment can be interpreted as the result of an effective, many-body directional entropic force [14] arising from the increased number of configurations available to the entire system, causing suitably faceted polyhedra to order. This notion of directional entropic forces and their relation to particle faceting suggests that particle shape can be used to predict assembled structures. To establish clear quantitative trends, however, requires data on many different shapes. We present thermodynamic Monte Carlo simulations of the self-assembly of 145 different polyhedra, including all the Platonic, Archimedean, Catalan and Johnson solids and some zonohedra, prisms, and antiprisms and show that we can use particle shape to predict the general category of ordered structure that forms.

Fig. 4.1 shows the polyhedra simulated, classified according to the structure(s) they assemble into from the dense fluid. The names of each polyhedron simulated and additional details can be found in Fig. 4.5 and Table 4.1 [21]. We group polyhedra into three assembly categories [12]: (i) crystals, (ii) plastic crystals, and (iii) liquid crystals. Polyhedra that are not observed to order are grouped as (iv) disordered (glasses). The categories are further subdivided into classes based on the type of order and crystallographic symmetry. All structures reported form repeatedly from disordered fluid phases at packing fractions between 0.49 and 0.63, depending on particle shape. We first note that $101/145 \approx 70\%$ of the polyhedra simulated assemble on the time scale of our simulations demonstrating a strong propensity for order in systems of polyhedra, even in the absence of explicit attractive interactions.

For crystals, we find five different Bravais lattices (hexagonal, cubic, body-centered tetragonal (BCT), rhombohedral, orthorhombic). The lattice shear we find with truncated cubes has been observed in experiments [13,22,23]. The A5 lattice, graphite structure, honeycomb lattice, diamond structure [14], and "supercube" lattice are periodic and have only a few particles in the unit cell. The quasicrystals have been reported previously with tetrahedra [11] and triangular bipyramids [24]. A new type of hexagonal random tiling forming independent layers is observed for the bilunabirotunda, a two-dimensional version of the random tiling seen in a molecular network [25].

Fig. 4.2 demonstrates both the diversity and structural complexity by showing

representative structures assembled by 12 polyhedra. Four examples of crystals are analyzed in more detail. Dürer's solids form a simple cubic crystal (Fig. 4.2A), which is unusual because it is a degenerate crystal [26]. Particles align randomly in four equivalent orientations. The space-filling gyrobifastigium assembles into a crystal isostructural to β-Sn, the metallic form of tin (Fig. 4.2B). Six square pyramids assemble into cubes ("supercubes") and then into a slightly sheared simple cubic lattice (Fig. 4.2C). The supercubes demonstrate the possibility of hierarchical assembly, similarly to an face-centered cubic (FCC) crystal reported for paired hemispheres [27]. Pentagonal orthobicupola have a disk-like shape and arrange with their five-fold symmetry axes aligned into the β-U crystal with the tiling $(3.4.3^2.4)$. A periodic approximant to a dodecagonal quasicrystal, this tiling is known as the sigma-phase and has been observed in micelles [28,29] and colloids [30], but with different decoration of the tiles (Fig. 4.2D)

We find that 66 of the 145 polyhedra crystallize into plastic crystals (rotator phases, [31]), in which the particles are free to rotate about their lattice positions. The plastic crystals we find all correspond to the crystallographically dense packings FCC (or hexagonally close-packed, HCP), body-centered cubic (BCC) and three topologically close-packed (TCP) polytetrahedral structures isostructural to β-W, β-Mn, and γ-brass. We do not distinguish between FCC and HCP, because simulations of these structures often contain high densities of stacking faults. In a TCP structure lattice sites are coordinated by distorted tetrahedra. We always observe plastic crystals for these three types of crystals.

In Fig. 4.2E we show that rhombic dodecahedra (the Voronoi cell of FCC) order into an FCC plastic crystal. We observe that the plastic crystal transforms into a non-rotator phase at higher packing fractions. Elongated triangular cupolas assemble a plastic BCC crystal (Fig. 4.2F). The formation of a high-symmetry phase is counter-intuitive given the asymmetric shape of the cupola. The paradiminished rhombicosidodecahedron has two large parallel faces and forms a plastic TCP phase isostructural to β-W (Fig. 4.2G). This phase, also known as the A15 structure, is frequently observed with micelles [32]. Dodecahedra assemble into the complex β-Mn structure (Fig. 4.2H). Since the distribution of Bragg peaks in the diffraction pattern resembles eight-fold symmetry, β-Mn can be interpreted as an approximant of an octagonal quasicrystal [33]. Indeed, we often observe 8-fold symmetry in the diffraction pattern during crystallization at an intermediate stage.

Truncated dodecahedra form γ-brass (Fig. 4.2I). With 52 atoms per unit cell it is the most complex periodic crystal observed in this study.

A nematic liquid crystal is formed by the pentagonal pyramid, which has a platelet-like shape (Fig. 4.2J). The up/down orientation of the pyramid relative to the director is random. The elongated square pyramid assembles into smectic layers (Fig. 4.2K). We confirmed there is no preferred orientation or long-range translational order within the layers. Like all regular prisms and antiprisms with five-fold or higher symmetry, the pentagonal prism assembles a columnar phase [34]. Particles are free to both shift along and rotate around the column axis (Fig. 4.2L).

44 polyhedra never self-assemble into an ordered structure on the time scale of our simulations, despite run times more than an order of magnitude longer than that needed for the slowest crystal former. Instead, the particle dynamics becomes gradually slower with increasing packing fraction, eventually producing a glassy state without discernible rotational or translational order. Because studies of dense packings of these polyhedra [34] yield crystals with higher packing fractions, we expect that the 44 particles are not intrinsic glass formers and instead have ordered "ground states" in the limit of infinite pressure. As in other examples [11,24], those ordered states may not be kinetically accessible in experiments. It is interesting to note that 41 of the 44 glass formers are Johnson solids and most are non-centrally symmetric. Johnson solids are typically less symmetric than Platonic and Archimedean solids, which all order in our simulations. This agrees with the intuition that highly symmetric polyhedra might be more easily assembled than non-symmetric ones. A complete investigation of assembly kinetics and propensity requires a careful analysis of the equations of state [10,15,24,35]. Preliminary data suggest that particles from the same assembly category have a comparable entropy gain ΔS at the transition. For instance, liquid crystals have $\Delta S = (1.8\pm0.5)k_B$ and plastic crystals $\Delta S = (1.0\pm0.5)k_B$. No clear trend is observed for shapes that assemble into crystals.

Several parameters have been used in the literature to analyze the shape of polyhedra [12,19,34]. A parameter that is sufficiently sensitive to large shape changes, but not too sensitive to small deformations, is the isoperimetric quotient, defined as IQ = $36pV^2/S^3$, where V is volume and S is surface area [36,37]. IQ can be calculated easily from the vertex vectors, and is closely related to the shape factor used in equations of state of

hard convex bodies [38]. A second parameter, the coordination number CN_f, accounts for the local arrangement of particles in the fluid phase prior to crystallization. In the case of glasses, we measure the coordination number at packing fraction 55%, which is the packing fraction where we typically observe crystallization of polyhedra that do not form glasses.

A correlation between the parameters IQ and CN_f and the assembly categories of Fig. 4.1 can be seen in Fig. 4.3A. We divide the parameter space into three regions. In the rightmost region (IQ > 0.7), 58 of 59 highly spherical polyhedra are observed to form plastic crystals. In the bottommost region (CN_f < 2), 21 of 24 polyhedra with few neighbors form liquid crystals. Finally, 16 of 18 particles in the center region (IQ ≤ 0.7 and CN_f ≥ 2) assemble into crystals. Thus, based on IQ and CN_f alone, the assembly of 95/101 = 94% of the polyhedra studied into crystals, liquid crystals or plastic crystals is explained. The outliers either lie within boundaries between regions, or they are nearly space-filling, favoring crystals over liquid or plastic crystals. We expect the shaded regions in Fig. 4.3A to become further refined as additional shapes are investigated. For example, the liquid crystal region is expected to expand upwards for prolate particles (not studied here), which have a higher CN than oblate particles while still having a low IQ.

We compare the coordination number measured close to the ordering transition in the fluid (CN_f) and in the ordered structure (CN_o) in Fig. 4.3B. Both numbers are nearly identical for almost all 101 shapes that assemble. This explains why it is sufficient to determine the coordination number in the dense fluid, which can be obtained from short simulations and experiments by integrating over the first peak of the radial distribution function, to predict with reasonable accuracy the category of structure that will form from the disordered fluid. As an independent test of 4. 3A, we calculated the IQ and CN for the family of truncated tetrahedra studied in Ref. [14] and correctly predict that each member should form a crystal (Fig. 4.6).

When comparing our observations with known crystal structures of atoms and molecules, which can be rationalized in terms of a few parameters like the strength and directionality of bonds between atoms [39] and the molecular geometry [40], we can interpret our findings as follows. First, FCC (HCP), and BCC crystals form from highly spherical polyhedra that have non-directional or weakly directional entropic interactions. TCP

structures are a compromise between high density and maintaining icosahedral local order present in the dense liquid. The coordination geometry can be visualized with Voronoi cells (Fig. 4.4A,B). Voronoi cells of TCP structures often have pentagonal or hexagonal faces. We frequently find TCP structures with particles that resemble the Voronoi cells, such as the (truncated) dodecahedron. The assembly of plastic crystals is dominated by packing, and their atomic analogue is metals and metallic bonding. It is interesting to note that all of our plastic crystals except γ-brass are isostructural to crystals found in elementary metals. Second, polyhedra that form crystals are more aspherical, with more pronounced and fewer faces. The crystal lattice is well represented by an ordered network of entropic "bonds" (Fig. 4.4C,D). Polyhedra assembling into crystals do not always resemble the Voronoi cells of the crystal, but usually have strong directional entropic bonding, reminiscent of covalent bonds. Third, polyhedra forming liquid crystals typically have an axial shape. Alignment of the most prominent faces is important for these phases and can be analyzed by the alignment of the directors (Fig. 4.4E,F). In general, we expect for axial particles to align prominent faces and long particle dimensions first. The behavior of polyhedra forming liquid crystals corresponds most closely to molecular liquid crystals. In all cases, the degree of directional entropic bonding may be quantified through various shape descriptors and correlation functions (Fig. 4.7).

Our results push the envelope of entropic crystallization and the assembly behavior of hard particle fluids, and provide an important step towards a predictive science of nanoparticle and colloidal assembly, which will be necessary to guide experiments with families of polyhedrally-shaped particles that are now becoming available. Although we are not yet able to predict a specific structure (e.g. BCC or diamond), the knowledge that obtaining, e.g., the diamond structure requires a shape with intermediate IQ or that a complex, topologically close-packed structure like g-brass requires a shape with high IQ provides important predictive guidance for building block design and synthesis. With further developments, more refined future structure prediction, with the level of detail now possible for atoms [41], should be attainable.

Additional Models and Methods

Polyhedra. The 145 convex polyhedra included in this study were chosen for their high

symmetry. They are the Platonic solids (#P01-P05, regular and identical faces), Archimedean solids (#A01-A13, regular faces with identical vertices), Catalan solids (#C01-C13, dual of the Archimedean solids), Johnson solids (#J01-J92, regular faces without identical faces), and other symmetric polyhedra (#O01-O22, including prisms, antiprisms and zonohedra). The polyhedron ID consists of a letter and a number. The letter stands for the group to which the polyhedron belongs: Platonic solid (P), Archimedean solid (A), Catalan solid (C), Johnson solid (J). Any other polyhedron not part of those four groups is labeled 'other' (O). The numbers enumerate the members in each group. We follow the ordering of regular polyhedra by Johnson [42] for Platonic, Archimedean, and Johnson solids. The Catalan solid #Cn is dual to the Archimedean solid #An. Standard ordering of the 'other symmetric polyhedra' #O is not found in the literature. In the case of prisms and antiprisms the edge length is chosen to be the same for all edges. A detailed list of the polyhedra and some of their geometric and assembly properties is given in Fig. 4.5 and Table 4.1.

Assembly behavior of a family of truncated tetrahedra. We tested the predictive ability of the IQ vs. CN plot of Fig. 4.3A for a family of truncated tetrahedra (Fig. 4.6A) recently studied in Ref. [14]. The two parameters isoperimetric quotient (IQ) and coordination number (CN) are determined as a function of truncation (Fig. 4.6B). We observe that, without exception, the members of the family fall into the region where crystals are expected. Indeed, Damasceno et al. [14] reported that truncated tetrahedra form five different crystal phases as a function of truncation.

Note that the coordination number jumps from $CN \approx 4$ for low truncation (tetrahedron-like) and intermediate truncation to $CN \approx 14$ for high truncation (octahedron-like). We analyze the jump using the radial distribution function (RDF) shown in Fig. 4.6C. As expected, the RDF varies smoothly within the stability regions for each phase, but behaves discontinuously at transitions between phases. In the stability regimes of diamond, β-tin, and high-pressure lithium the gap between the first and the second peak of the RDF closes gradually. At the transition to the rhombohedral phase, the equilibrium phase for octahedra, and the two peaks merge and form a single peak. The result is a jump in the coordination number.

In the case of the 145 polyhedra studied in the main text, the possibility of RDF peak merging and splitting explains the occurrence of crystals in two regions corresponding to high and low CN, respectively (see Fig. 4.3A). For intermediate CN ($8 \leq CN \leq 12$), no phases are observed. We speculate that the fusion/split mechanism of RDF peaks might be a general mechanism and indicate this in Fig. 4.3A and Fig. 4.6B by shading the middle region with a lower intensity.

It was remarked[14] that octahedra can form a BCC plastic crystal close to melting, which is metastable to a rhombohedral crystal by only a small free energy difference [15]. The appearance of the BCC plastic crystal competing with a crystal phase is expected, because the IQ value of octahedra is close to that typical for the plastic crystal region in Fig. 4.6B. In fact, we would predict that a further rounding of the octahedron would completely stabilize the BCC rotator phase. Indeed, this is precisely the case as found recently in a study of 'rounded octahedra' (superballs) by Ni et al. [15].

Local order and entropic bonding

We analyze the local order in the assembled structures and the role of entropic bonding in more detail using a shape descriptor given by the distribution of the face normal vectors of the particle on the sphere, weighted by the face area. This is a good descriptor to characterize directional entropic forces because face normal vectors indicate the directions in which we expect the alignment of neighboring faces by entropic "bonds". A second shape descriptor – the bond order diagram of nearest neighbors – measures the actual direction of "bonds" as found during the simulation. Similarity of the two measures indicates a direct relation between particle shape and local order. The relative orientation of the neighbors is analyzed using orientational correlation diagrams (see Methods), which are sensitive to rotations that change the degree of alignment, but not to rotations around the bonds. Peaks are expected in the orientational correlation diagram if face-to-face alignment persists over time, and a uniform intensity if it does not.

Polyhedra that form plastic crystals (Fig. 4.7A) often have many small faces; consequently, the shape descriptor exhibits many peaks in all directions. Indeed, bond directions are only weakly correlated with face normals. Also, the orientational correlation diagram is isotropic, as expected if face-to-face alignment is not a factor. This shows that

directional entropic forces are not important for plastic crystals. To first approximation, polyhedra that form plastic crystals assemble into crystal structures known to be good sphere packings. Highly spherical particles form the densest sphere packings FCC and HCP. TCP phases are a compromise between high density and maintaining icosahedral local order present in the dense liquid.

Polyhedra that form crystals (Fig. 4.7B) are more aspherical with more pronounced, and fewer, faces. We find a strong correlation between the bond order diagram and the direction of face normal vectors, which demonstrates that face-to-face alignments dominate.

Polyhedra forming liquid crystals (Fig. 4.7C) typically have an axial shape, which is reflected in the shape descriptor by the dominance of a few faces. Bond order diagrams and orientational correlation diagrams of nematics and smectics exhibit continuous rotational symmetry. We observe that particles can form bonds in certain directions, but often rotate freely around these bonds. Additionally, we can also distinguish trends among liquid crystals: shapes forming discotic liquid crystals are dominated by two parallel faces, which induces columnar stacking; in smectic phases, the rotation around the prominent faces is frustrated and, rather than columns, the particles instead order into layers, where they can freely translate; in nematic liquid crystals, stacking is further disfavored by the lack of prominent parallel faces and the particles merely align without translational order, exchanging rotational degrees of freedom for translational entropy.
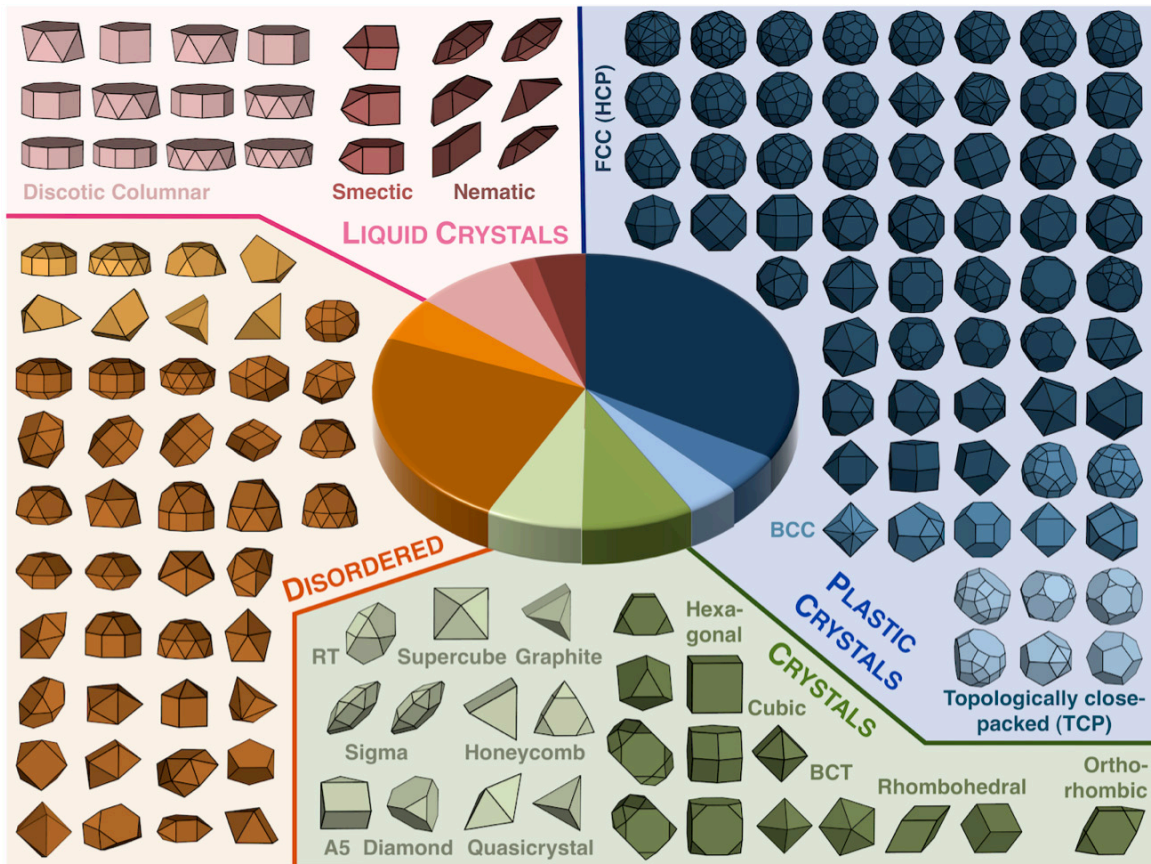
Figure 4.1. Hard particle classification according to their assembly. Polyhedra are separated into four categories of organization as indicated by different colors: liquid crystals, plastic crystals, crystals, and disordered (glassy) phases. Subcategories (classes) are indicated by shades. The assembly category of liquid crystals contains the classes discotic columnar, smectic, and nematic (different shades of pink). Plastic crystal classes are face-centered cubic (dark blue), body-centered cubic (blue), and topologically close packed (light blue). In the case of crystals, we distinguish Bravais lattices (dark green) and non-Bravais lattices (light green). RT stands for random tiling. For the glasses, no assembly is observed, and we distinguish those that strongly order locally with preferential face-to-face alignment (light orange) from those with only weak local order (dark orange). The pie chart in the center compares the relative frequency of the ten observed classes. In each of the classes, polyhedra are listed in decreasing order of the isoperimetric quotient. A polyhedron is included multiple times if it was found to assemble into more than one ordered structure.
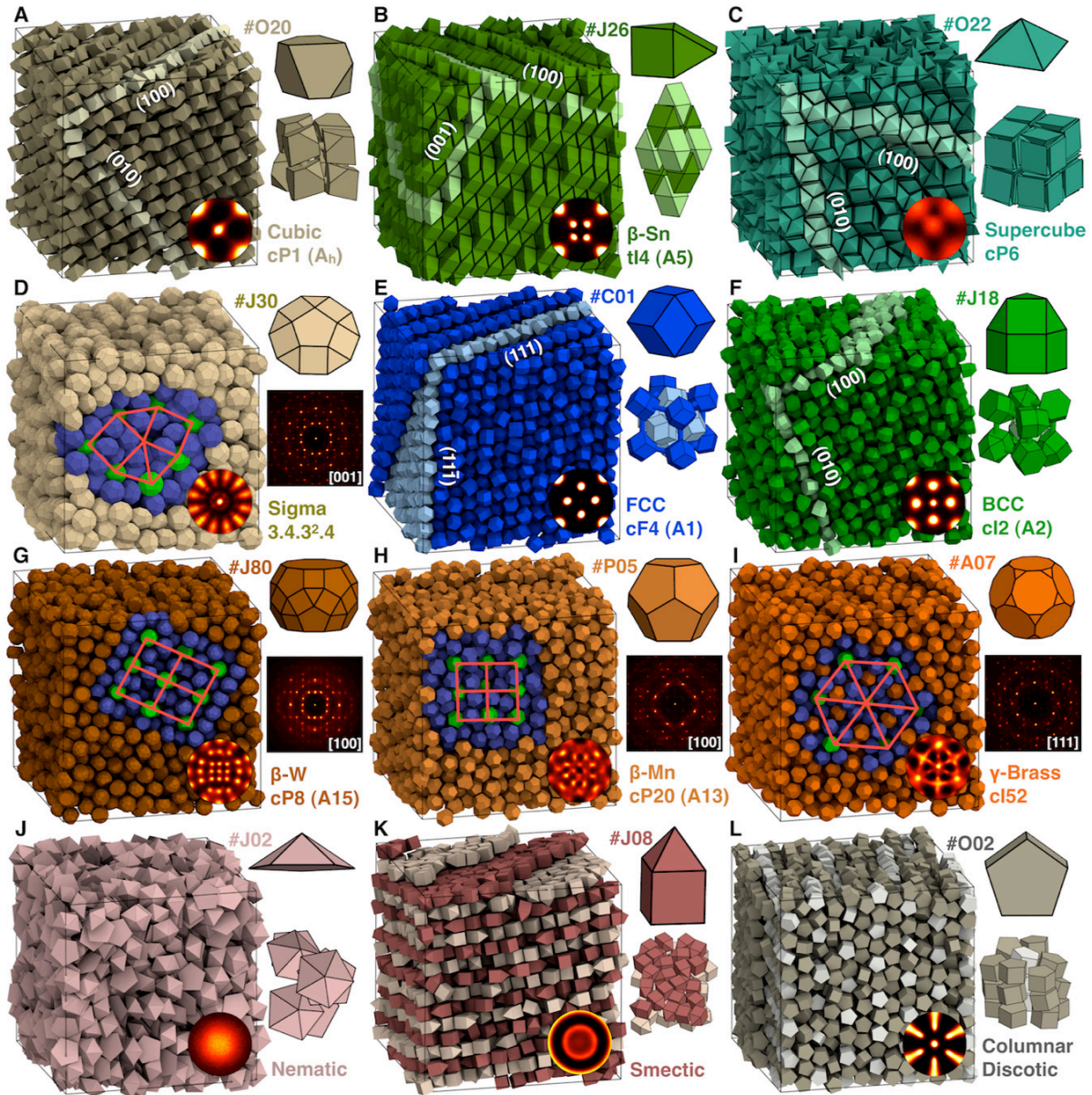
Figure 4.2. Examples of structures assembled from hard particles. Systems of 2048 polyhedra were assembled starting from the disordered fluid. In each subfigure, a snapshot of the simulation box (left), the bond-order diagram for nearest neighbors (inset), the polyhedron shape and ID (top right), a small group of particles or the diffraction pattern (middle right), and the crystallographic characterization consisting of name or atomic prototype, Pearson symbol and Strukturbericht designation (bottom right) are shown. The snapshots depict crystals (**A-D**), plastic crystals (**E-I**), and liquid crystals (**J-L**). Some low index planes (**A-C, E, F**), tilings descriptions consisting of squares and triangles (**D, G-I**) and structural features (**K**, **L**) are highlighted in the simulation snapshots by different colors.
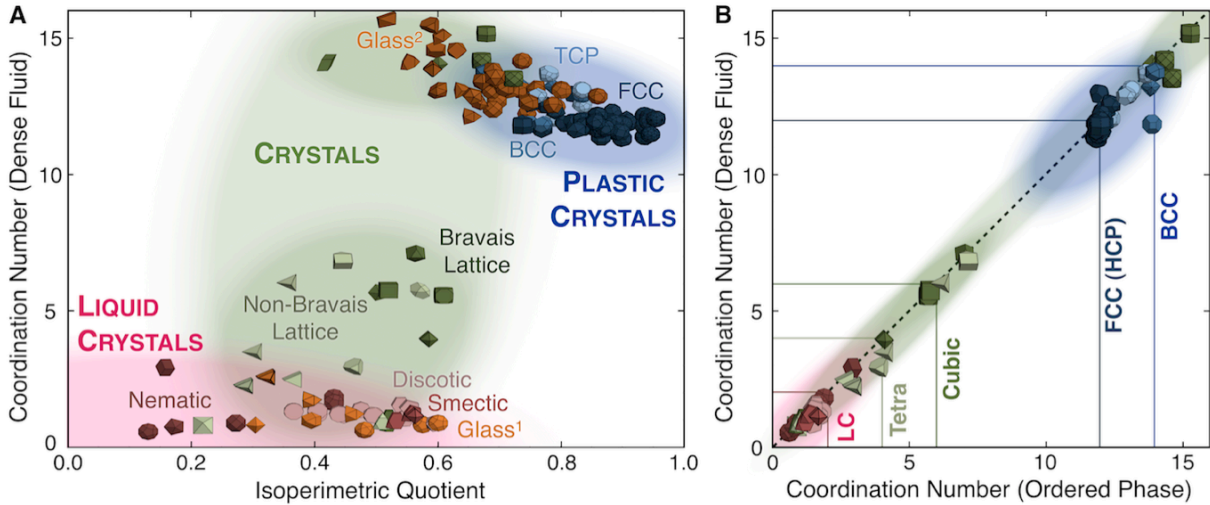
Figure 4.3. Assembly of polyhedra into different crystalline classes. (**A**) The coordination number in the fluid phase, CN_f, is correlated to the isoperimetric quotient (IQ) of the polyhedron. Here, IQ is a scalar parameter for the sphericity of the shape and coordination number is a measure for the degree of local order. Data points are drawn as small polyhedra. Polyhedra are colored and grouped according to the assemblies they form. (**B**) Polyhedra have, in most cases, nearly identical coordination number in the ordered phase (CN_o) and the fluid phase (CN_f) close to the ordering transition. Because of this strong correlation, combining CN_f and IQ allows for prediction of the assembly category expected for most cases.
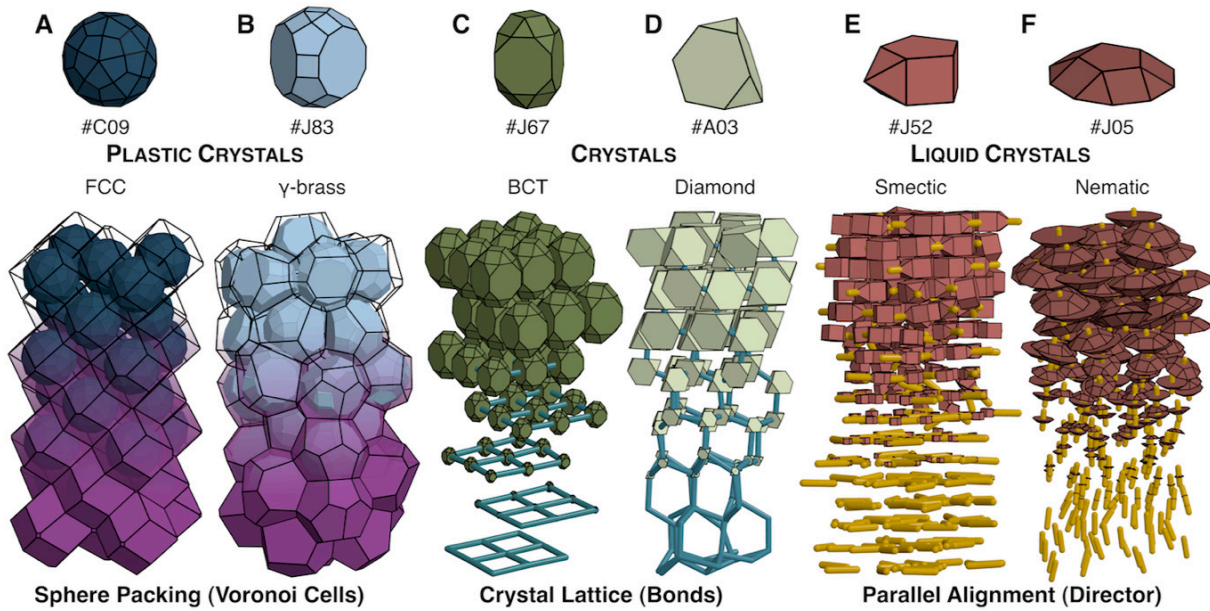
Figure 4.4. Systems of assembled polyhedra and their bond types. Polyhedra and their IDs are shown at top and small groups of particles are extracted from simulation snapshots below. (**A**,**B**) In plastic crystals, polyhedra rotate inside their Voronoi cells. (**C**,**D**) Entropic "bonds" in the direction of the face normal are important for crystals. (**E**,**F**) Parallel alignment dominates in the case of liquid crystals. From top to bottom, the transparency of Voronoi cells is decreased and/or the size of polyhedra is reduced.
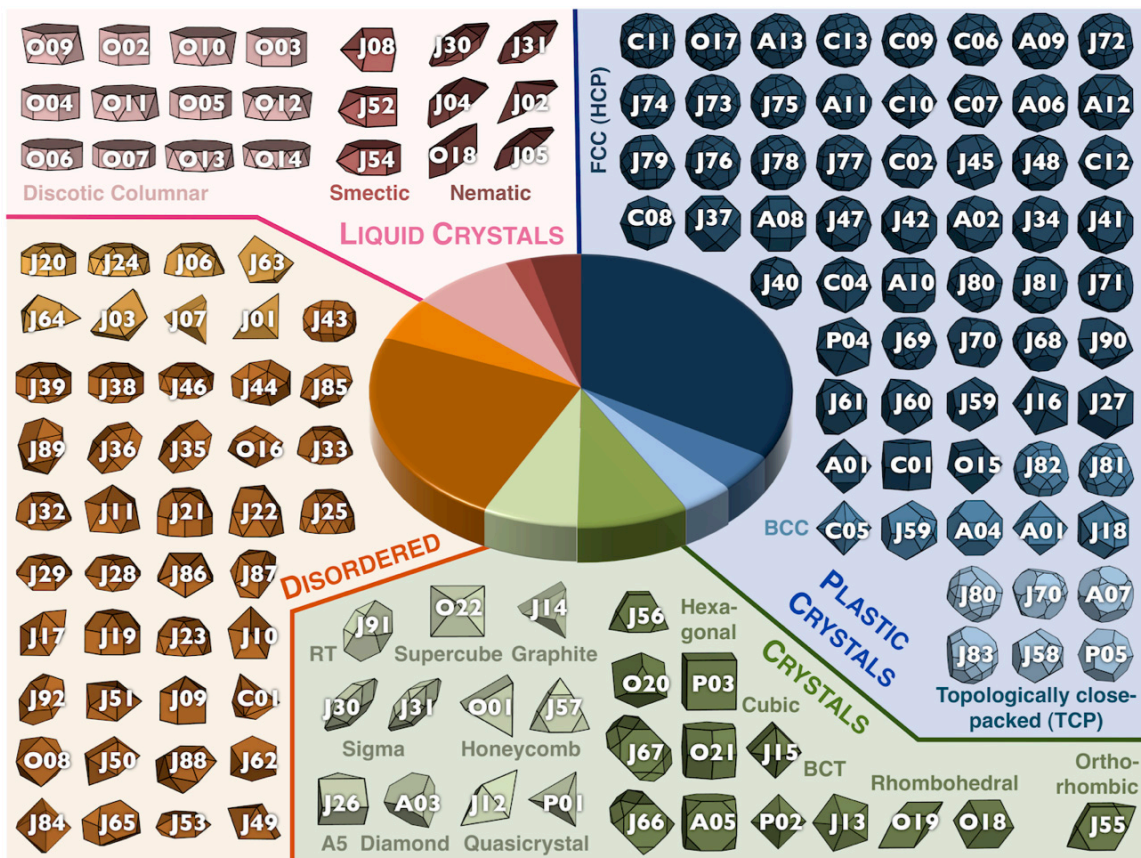
Figure 4.5. Identifiers (IDs) of the 145 polyhedra studied in this work. Each ID consists of a letter and a number. The letter stands for the group of polyhedron: Platonic solid (P), Archimedean solid (A), Catalan solid (C), Johnson solid (J). Any other polyhedron is labeled 'other' (O). The numbers enumerate the members in each group. The full names of the polyhedra are given in Table 4.1.
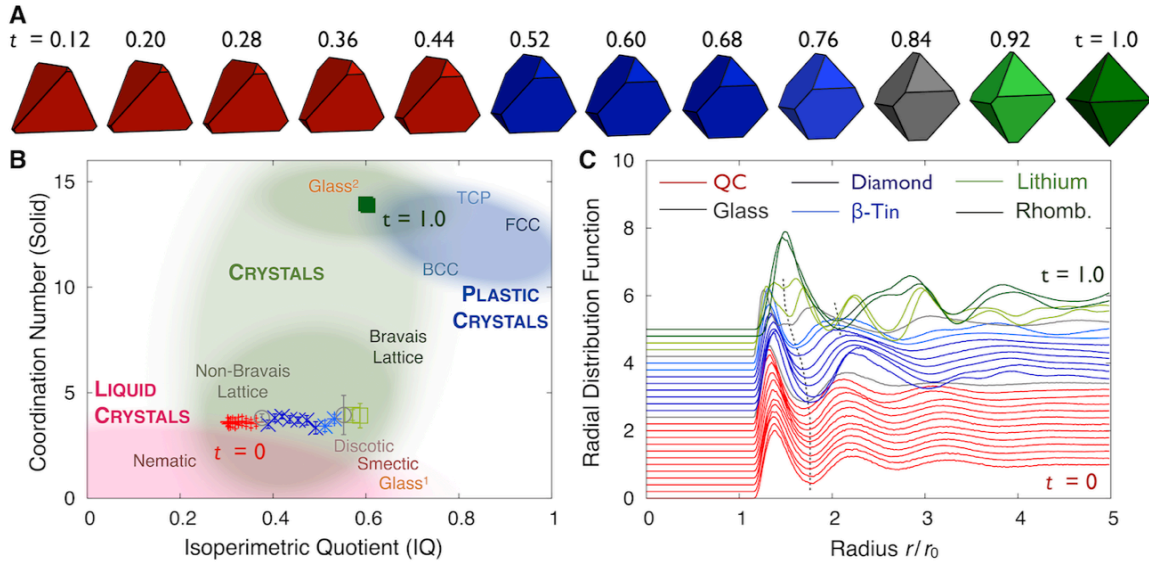
Figure 4.6. Predicted and observed structures for a family of truncated tetrahedra. (**A**) With increasing truncation the shape interpolates between a regular tetrahedron and a regular octahedron. Five assembled phases were reported [14]. The phases are indicated by color: dodecagonal quasicrystal (red), diamond (dark blue), β-tin (blue), high-pressure lithium (green), and a rhombohedral Bravais lattice (dark green). (**B**) The family is mapped onto the IQ vs. CN plot of Fig. 4.3A. With increasing truncation the isoperimetric quotient increases from IQ = 0.3 to IQ = 0.6. The coordination number stays constant at CN ≈ 4 for truncation t < 0.94, and jumps up to CN = 14 for t > 0.94. (**C**) The radial distribution function shows discontinuities at transitions between phases. A particularly strong discontinuity occurs at t = 0.94 coinciding with the jump in CN. As an octahedral shape is approached, the first and second coordination shells fuse at the jump to form a single new first coordination shell. For viewing purposes, radial distribution functions are shown shifted by constant values with increasing truncation.
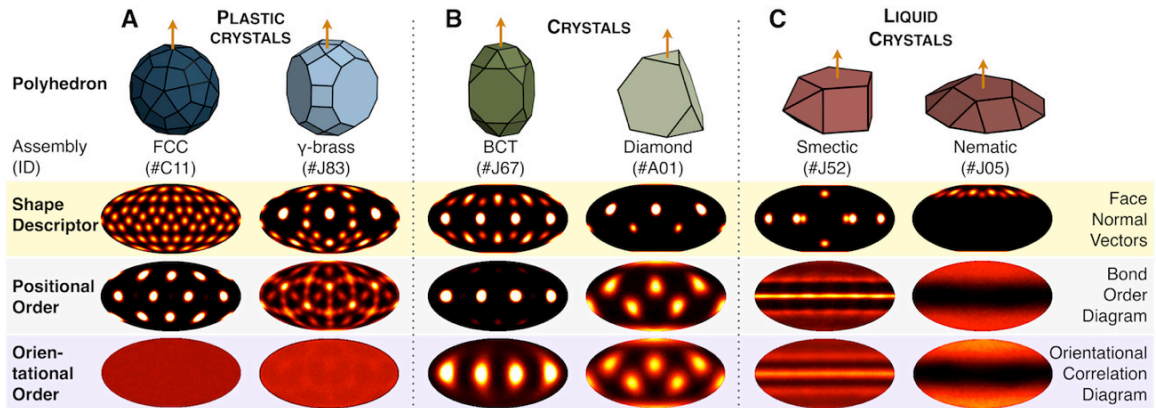
Figure 4.7. Relation between particle shape and entropic "bonds". We analyze six systems of polyhedra that span the three assembly categories observed with hard polyhedra. Polyhedra and their IDs are shown at top. The distribution of face normal vectors, the bond order diagram, and orientational correlation diagrams (the latter two for nearest neighbors) are measures for the shape, positional local order and orientational local order, respectively. The diagrams demonstrate that entropic bonds are weak in plastic crystals (**A**), strong in crystals (**B**), and highly axial in liquid crystals (**C**).

Platonic Solids					
ID	**Name of the polyhedron**	**IQ**	**Structure(s)**	**CN$_f$**	**CN$_o$**
P01	Tetrahedron	0.302	Dodecagonal Quasicrystal	3.5	4.1
P02	Octahedron	0.605	Rhombohedral (densest packing)	14.0	13.9
P03	Cube (space filling: simple cubic)	0.524	Cubic (densest packing)	5.8	5.8
P04	Icosahedron	0.829	FCC	11.6	11.9
P05	Dodecahedron	0.755	Beta-Mn	13.0	13.1

Archimedean Solids					
ID	**Name of the polyhedron**	**IQ**	**Structure(s)**	**CN$_f$**	**CN$_o$**
A01	Cuboctahedron	0.741	FCC + BCC	13.3	12.0
A02	Icosidodecahedron	0.860	FCC	11.7	12.0
A03	Truncated Tetrahedron	0.466	Diamond	3.0	3.9
A04	Truncated Octahedron (space filling: BCC)	0.753	BCC	11.8	13.9
A05	Truncated Cube	0.613	Rhombohedral (densest packing)	5.6	5.7
A06	Truncated Icosahedron	0.903	FCC	11.3	11.9
A07	Truncated Dodecahedron	0.794	Gamma-Brass	12.1	12.4
A08	Rhombicuboctahedron	0.868	FCC	11.4	11.8
A09	Rhombicosidodecahedron	0.939	FCC	11.8	11.9
A10	Truncated Cuboctahedron	0.839	FCC	12.0	12.0
A11	Truncated Icosidodecahedron	0.914	FCC	11.9	12.0
A12	Snub Cuboctahedron	0.899	FCC	11.6	11.9
A13	Snub Icosidodecahedron	0.947	FCC	12.1	12.1

Catalan Solids					
ID	**Name of the polyhedron**	**IQ**	**Structure(s)**	**CN$_f$**	**CN$_o$**
C01	Rhombic Dodecahedron (space filling: FCC)	0.740	FCC	11.8	12.0
C02	Rhombic Triacontahedron	0.887	FCC	12.3	12.0
C03	Triakis Tetrahedron	0.646	Disordered	13.1	
C04	Tetrakis Hexahedron	0.843	FCC	11.8	11.9
C05	Triakis Octahedron	0.790	BCC	13.2	13.8
C06	Pentakis Dodecahedron	0.940	FCC	11.4	11.8
C07	Triakis Icosahedron	0.905	FCC	11.9	11.8
C08	Deltoidal Icositetrahedron	0.870	FCC	11.9	12.0
C09	Deltoidal Hexecontahedron	0.946	FCC	12.0	11.9
C10	Disdyakis Dodecahedron	0.910	FCC	12.0	12.0

C11	Disdyakis Triacontahedron	0.958	FCC	12.0	12.1
C12	Pentagonal Icositetrahedron	0.873	FCC	11.6	12.0
C13	Pentagonal Hexecontahedron	0.946	FCC	11.9	12.0

Johnson Solids					
ID	**Name of the polyhedron**	**IQ**	**Structure(s)**	**CN_f**	**CN_o**
J01	Pyramid 4 (Square Pyramid)	0.308	Disordered (dimers)	0.8	
J02	Pyramid 5	0.175	Nematic	0.8	0.8
J03	Triangular Cupola	0.399	Disordered (dimers)	1.0	
J04	Square Cupola	0.276	Nematic	0.9	0.9
J05	Pentagonal Cupola	0.134	Nematic	0.6	0.6
J06	Pentagonal Rotunda	0.485	Disordered (dimers)	0.6	
J07	Elongated Triangular Pyramid	0.324	Disordered (dimers)	2.6	
J08	Elongated Square Pyramid	0.566	Smectic	1.2	1.7
J09	Elongated Pentagonal Pyramid	0.659	Disordered	12.9	
J10	Gyroelongated Square Pyramid	0.676	Disordered	13.4	
J11	Gyroelongated Pentagonal Pyramid	0.721	Disordered	13.1	
J12	Dipyramid 3 (Triangular Dipyramid)	0.358	Dodecagonal Quasicrystal	6.0	6.1
J13	Dipyramid 5 (Pentagonal Dipyramid)	0.507	Rhombohedral (densest packing)	5.7	5.7
J14	Elongated Triangular Dipyramid	0.288	Graphite (densest packing)	2.3	2.9
J15	Elongated Square Dipyramid	0.589	BCT (densest packing)	4.0	4.1
J16	Elongated Pentagonal Dipyramid	0.752	FCC	12.6	12.4
J17	Gyroelongated Square Dipyramid	0.694	Disordered	13.8	
J18	ElongatedTriangularCupola	0.681	BCC	13.7	14.0
J19	Elongated Square Cupola	0.693	Disordered	12.4	
J20	Elongated Pentagonal Cupola	0.604	Disordered (dimers)	0.9	
J21	Elongated Pentagonal Rotunda	0.713	Disordered	13.2	
J22	Gyroelongated Triangular Cupola	0.711	Disordered	13.1	
J23	Gyroelongated Square Cupola	0.690	Disordered	13.1	
J24	Gyroelongated Pentagonal Cupola	0.579	Disordered (dimers)	0.8	
J25	Gyroelongated Pentagonal Rotunda	0.709	Disordered	13.4	
J26	Gyrobifastigium (space filling: A5)	0.450	A5 (densest packing)	6.9	7.2
J27	Triangular Orthobicupola	0.741	FCC	11.9	12.1
J28	Square Orthobicupola	0.700	Disordered	12.7	12.7

J29	Square Gyrobicupola	0.700	Disordered	12.7	12.7
J30	Pentagonal Orthobicupola	0.435	Nematic + Sigma	1.8	1.9
J31	Pentagonal Gyrobicupola	0.435	Nematic + Sigma	1.6	1.7
J32	Pentagonal Orthocupolarotunda	0.741	Disordered	13.1	
J33	Pentagonal Gyrocupolarotunda	0.741	Disordered	14.2	
J34	Pentagonal Orthobirotunda	0.860	FCC	11.9	11.8
J35	Elongated Triangular Orthobicupola	0.751	Disordered	12.6	
J36	ElongatedTriangular Gyrobicupola	0.751	Disordered	12.7	
J37	Elongated Square Gyrobicupola	0.868	FCC	11.5	11.9
J38	Elongated Pentagonal Orthobicupola	0.804	Disordered	13.1	
J39	Elongated Pentagonal Gyrobicupola	0.804	Disordered	13.1	
J40	Elongated Pentagonal Orthocupolarotunda	0.860	FCC	11.9	12.0
J41	Elongated Pentagonal Gyrocupolarotunda	0.860	FCC	12.0	12.0
J42	Elongated Pentagonal Orthobirotunda	0.863	FCC	12.2	12.0
J43	Elongated Pentagonal Gyrobirotunda	0.863	Disordered	12.9	
J44	Gyroelongated Triangular Bicupola	0.791	Disordered	12.6	
J45	Gyroelongated Square Bicupola	0.887	FCC	11.9	12.1
J46	Gyroelongated Pentagonal Bicupola	0.796	Disordered	12.5	
J47	Gyroelongated Pentagonal Cupolarotunda	0.866	FCC	11.6	11.9
J48	Gyroelongated Pentagonal Birotunda	0.876	FCC	11.7	11.9
J49	Augmented Triangular Prism	0.520	Disordered	15.7	
J50	Biaugmented Triangular Prism	0.611	Disordered	15.0	
J51	Triaugmented Triangular Prism	0.660	Disordered	13.7	
J52	Augmented Pentagonal Prism	0.561	Smectic	1.3	1.4
J53	Biaugmented Pentagonal Prism	0.559	Disordered	14.1	
J54	Augmented Hexagonal Prism	0.535	Smectic	1.0	1.2
J55	Parabiaugmented Hexagonal Prism	0.525	Orthorhombic	0.9	0.9
J56	Metabiaugmented Hexagonal Prism	0.525	Hexagonal	1.1	1.1
J57	Triaugmented Hexagonal Prism	0.514	Honeycomb	1.0	1.0
J58	Augmented Dodecahedron	0.765	Beta-Mn	12.9	12.9
J59	Parabiaugmented Dodecahedron	0.774	FCC + BCC	11.8	12.0
J60	Metabiaugmented Dodecahedron	0.774	FCC	11.6	11.9
J61	Triaugmented Dodecahedron	0.782	FCC	12.5	12.4
J62	MetabidiminishedIcosahedron	0.601	Disordered	14.6	
J63	Tridiminished Icosahedron	0.469	Disordered (dimers)	2.1	
J64	Augmented Tridiminished Icosahedron	0.400	Disordered (dimers)	2.4	
J65	Augmented Truncated Tetrahedron	0.590	Disordered	15.5	
J66	Augmented Truncated Cube	0.675	Rhombohedral	14.2	14.3
J67	Biaugmented Truncated Cube	0.726	BCT	13.5	14.6

ID	Name of the polyhedron	IQ	Structure(s)	CN$_f$	CN$_o$
			(densest packing)		
J68	Augmented Truncated Dodecahedron	0.809	FCC	11.9	11.9
J69	Parabiaugmented Truncated Dodecahedron	0.824	FCC	11.9	12.0
J70	Metabiaugmented Truncated Dodecahedron	0.824	FCC + Beta-Mn	12.9	11.9
J71	Triaugmented Truncated Dodecahedron	0.837	FCC	11.7	12.0
J72	Gyrate Rhombicosidodecahedron	0.939	FCC	11.8	11.9
J73	Parabigyrate Rhombicosidodecahedron	0.939	FCC	10.9	11.1
J74	Metabigyrate Rhombicosidodecahedron	0.939	FCC	12.2	12.2
J75	Trigyrate Rhombicosidodecahedron	0.939	FCC	11.4	11.9
J76	Diminished Rhombicosidodecahedron	0.890	FCC	11.8	12.0
J77	Paragyrate Diminished Rhombicosidodecahedron	0.890	FCC	11.6	11.9
J78	Metagyrate Diminished Rhombicosidodecahedron	0.890	FCC	11.9	12.0
J79	Bigyrate Diminished Rhombicosidodecahedron	0.890	FCC	11.6	11.9
J80	Parabidiminished Rhombicosidodecahedron	0.838	FCC + A15	12.5	12.3
J81	Metabidiminished Rhombicosidodecahedron	0.838	FCC + BCC	13.1	13.1
J82	Gyrate Bidiminished Rhombicosidodecahedron	0.838	BCC	12.9	13.0
J83	Tridiminished Rhombicosidodecahedron	0.784	Gamma-Brass	13.7	13.7
J84	Snub Disphenoid	0.596	Disordered	13.9	
J85	Snub Square Antiprism	0.771	Disordered	12.6	
J86	Sphenocorona	0.697	Disordered	13.5	
J87	Augmented Sphenocorona	0.696	Disordered	13.5	
J88	Sphenomegacorona	0.603	Disordered	13.1	
J89	Hebesphenomegacorona	0.763	Disordered	13.1	
J90	Disphenocingulum	0.795	FCC	12.3	12.2
J91	Bilunabirotunda	0.575	Hexagonal (random tiling)	5.7	5.7
J92	Triangular Hebesphenorotunda	0.671	Disordered	12.7	

Other Polyhedra					
ID	Name of the polyhedron	IQ	Structure(s)	CN$_f$	CN$_o$
O01	Triangular Prism (edge len. = 1) (space filling: honeycomb)	0.367	Honeycomb (densest packing)	2.5	2.6
O02	Pentagonal Prism (edge len. = 1)	0.557	Columnar	1.4	1.5
O03	Hexagonal Prism (edge len. = 1) (space filling: hexagonal)	0.544	Columnar	1.5	1.6
O04	Heptagonal Prism (edge len. = 1)	0.514	Columnar	1.0	1.4
O05	Octagonal Prism (edge len. = 1)	0.479	Columnar	1.4	1.7

O06	Nonagonal Prism (edge len. = 1)	0.443	Columnar	1.2	1.5
O07	Decagonal Prism (edge len. = 1)	0.409	Columnar	1.2	1.5
O08	Square Antiprism (edge len. = 1)	0.635	Disordered	14.5	
O09	Pentagonal Antiprism (edge len. = 1)	0.601	Columnar	0.9	1.5
O10	Hexagonal Antiprism (edge len. = 1)	0.551	Columnar	1.1	1.5
O11	Heptagonal Antiprism (edge len. = 1)	0.499	Columnar	1.2	1.7
O12	Octagonal Antiprism (edge len. = 1)	0.452	Columnar	1.2	1.7
O13	Nonagonal Antiprism (edge len. = 1)	0.409	Columnar	1.3	1.8
O14	Decagonal Antiprism (edge len. = 1)	0.370	Columnar	1.3	1.7
O15	Squashed Dodecahedron	0.740	FCC	11.8	12.0
O16	RhombicIcosahedron	0.749	Disordered	12.2	
O17	Rhombic Enneacontahedron	0.949	FCC	11.5	11.9
O18	Obtuse Golden Rhombohedron (space filling: rhombohedral)	0.162	Nematic + Rhombohedral	2.9	2.9
O19	Acute Golden Rhombohedron (space filling: rhombohedral)	0.424	Rhombohedral (densest packing)	14.1	14.1
O20	Duerers Solid	0.568	Cubic	7.1	7.0
O21	Elongated Dodecahedron (space filling: BCT)	0.682	BCT (densest packing)	15.2	15.3
O22	Square pyramid (height = 1/2 edge length) (space filling: supercube)	0.233	Supercube (densest packing)	0.8	0.9

Table 4.1. Assembly behavior of 145 polyhedra. Column 1: identifier; Column 2: full name; Column 3: isoperimetric quotient IQ; Column 4: all ordered structures found during compression when assembling the polyhedron from the disordered liquid; Column 5: coordination number CN_f in the fluid; Column 6: coordination number CN_o in the ordered phase. For glasses, we determine the coordination number at a packing fraction of 55%. The color indicates the category of organization that formed first (at lowest packing fraction) from the fluid: green = crystal; blue = plastic crystal; red = liquid crystal; orange = disordered. There are ten space-filling polyhedra: #P03, #A04, #C01, #J26, #O01, #O03, #O18, #O19, #O21, #O22. The space-filling tilings are included in the table. We add a note to column 4 in cases where the assembled phase is identical to that of the densest reported packing of the polyhedron in Ref. [15].

References for Chapter 4

(1)   Pauling, L. The Principles Determining the Structure of Complex Ionic Crystals. J. Am. Chem. Soc. **1929**, 51, 1010–1026.

(2)   Li, F.; Josephson, D. P.; Stein, A. Colloidal Assembly: The Road from Particles to Colloidal Molecules and Crystals. Angew. Chemie Int. Ed. **2011**, 50, 360–388.

(3)   Glotzer, S. C.; Solomon, M. J. Anisotropy of Building Blocks and Their Assembly into Complex Structures. Nat. Mater. **2007**, 6, 557–562.

(4)   Quan, Z.; Fang, J. Superlattices with Non-Spherical Building Blocks. Nano Today **2010**, 5, 390–411.

(5)   Huang, M. H.; Lin, P.-H. Shape-Controlled Synthesis of Polyhedral Nanocrystals and Their Facet-Dependent Properties. Adv. Funct. Mater. **2012**, 22, 14–24.

(6)   Alder, B. J.; Wainwright, T. E. Phase Transition for a Hard Sphere System. J. Chem. Phys. **1957**, 27, 1208–1209.

(7)   Eldridge, M. D.; Madden, P. A.; Frenkel, D. Entropy-Driven Formation of a Superlattice in a Hard-Sphere Binary Mixture. Nature **1993**, 365, 35–37.

(8)   Onsager, L. The Effects of Shape on the Interaction of Colloidal Particles. Ann. N. Y. Acad. Sci. **1949**, 51, 627–659.

(9)   Frenkel, D.; Lekkerkerker, H. N. W.; Stroobants, A. Thermodynamic Stability of a Smectic Phase in a System of Hard Rods. Nature **1988**, 332, 822–823.

(10)   Frenkel, D.; Mulder, B. M. The Hard Ellipsoid-of-Revolution Fluid. Mol. Phys. **1985**, 55, 1171–1192.

(11)   Haji-Akbari, A.; Engel, M.; Keys, A. S.; Zheng, X.; Petschek, R. G.; Palffy-Muhoray, P.; Glotzer, S. C. Disordered, Quasicrystalline and Crystalline Phases of Densely Packed Tetrahedra. Nature **2009**, 462, 773–777.

(12)   Agarwal, U.; Escobedo, F. a. Mesophase Behaviour of Polyhedral Particles. Nat. Mater. **2011**, 10, 230–235.

(13)   Henzie, J.; Grünwald, M.; Widmer-Cooper, A.; Geissler, P. L.; Yang, P. Self-Assembly of Uniform Polyhedral Silver Nanocrystals into Densest Packings and Exotic Superlattices. Nat. Mater. **2012**, 11, 131–137.

(14)   Damasceno, P. F.; Engel, M.; Glotzer, S. C. Crystalline Assemblies and Densest Packings of a Family of Truncated Tetrahedra and the Role of Directional Entropic Forces. ACS Nano **2011**, 6, 23.

(15)   Ni, R.; Gantapara, A. P.; de Graaf, J.; van Roij, R.; Dijkstra, M. Phase Diagram of Colloidal Hard Superballs: From Cubes via Spheres to Octahedra. Arxiv Prepr. arXiv **2011**, 2, 1–5.

(16)   Smallenburg, F.; Filion, L.; Marechal, M.; Dijkstra, M. Vacancy-Stabilized Crystalline Order in Hard Cubes. arXiv **2012**, 1111.4357, 1–5.

(17)   Rossi, L.; Sacanna, S.; Irvine, W. T. M.; Chaikin, P. M.; Pine, D. J.; Philipse, A. P. Cubic Crystals from Cubic Colloids. Soft Matter **2011**, 7, 4139.

(18)   Frenkel, D. Entropy-Driven Phase Transitions. Physica A **1999**, 263, 26–38.

(19)   Torquato, S.; Jiao, Y. Dense Packings of the Platonic and Archimedean Solids. Nature **2009**, 460, 876–879.

(20)   Young, K. L.; Jones, M. R.; Zhang, J.; Macfarlane, R. J.; Esquivel-Sirvent, R.; Nap, R. J.; Wu, J.; Schatz, G. C.; Lee, B.; Mirkin, C. a. Assembly of Reconfigurable One-

Dimensional Colloidal Superlattices due to a Synergy of Fundamental Nanoscale Forces. PNAS **2012**, 109, 2240–2245.

(21) Materials and Methods Are Available as Supporting Material on Science Online.

(22) Zhao, K.; Bruinsma, R.; Mason, T. G. Entropic Crystal-Crystal Transitions of Brownian Squares. Proc. Natl. Acad. Sci. U. S. A. **2011**, 108, 2684–2687.

(23) Zhang, Y.; Lu, F.; van der Lelie, D.; Gang, O. Continuous Phase Transformation in Nanocube Assemblies. Phys. Rev. Lett. **2011**, 107, 2–5.

(24) Haji-Akbari, A.; Engel, M.; Glotzer, S. C. Degenerate Quasicrystal of Hard Triangular Bipyramids. Phys. Rev. Lett. **2011**, 107, 1–5.

(25) Blunt, M. O.; Russell, J. C.; Giménez-López, M. D. C.; Garrahan, J. P.; Lin, X.; Schröder, M.; Champness, N. R.; Beton, P. H. Random Tiling and Topological Defects in a Two-Dimensional Molecular Network. Science (80-.). **2008**, 322, 1077–1081.

(26) Gerbode, S.; Lee, S.; Liddell, C.; Cohen, I. Restricted Dislocation Motion in Crystals of Colloidal Dimer Particles. Phys. Rev. Lett. **2008**, 101.

(27) Marechal, M.; Kortschot, R. J.; Demirörs, A. F.; Imhof, A.; Dijkstra, M. Phase Behavior and Structure of a New Colloidal Model System of Bowl-Shaped Particles. Nano Lett. **2010**, 10, 1907–1911.

(28) Ungar, G.; Liu, Y.; Zeng, X.; Percec, V.; Cho, W.-D. Giant Supramolecular Liquid Crystal Lattice. Science (80-.). **2003**, 299, 1208–1211.

(29) Lee, S.; Bluemle, M. J.; Bates, F. S. Discovery of a Frank-Kasper Sigma Phase in Sphere-Forming Block Copolymer Melts. Science (80-.). **2010**, 330, 349–353.

(30) Talapin, D. V; Shevchenko, E. V; Bodnarchuk, M. I.; Ye, X.; Chen, J.; Murray, C. B. Quasicrystalline Order in Self-Assembled Binary Nanoparticle Superlattices. Nature **2009**, 461, 964–967.

(31) Although "Rotator Phases" Constitute a Subset of "Plastic Crystals" in Molecular Materials, the Terms Are Used Synonymously for Hard Particles.

(32) Ziherl, P.; Kamien, R. D. R. D. Maximizing Entropy by Minimizing Area: Towards a New Principle of Self-Organization. J. Phys. Chem. B **2001**, 105, 10147–10158.

(33) Elenius, M.; Zetterling, F.; Dzugutov, M.; Fredrickson, D.; Lidin, S. Structural Model for Octagonal Quasicrystals Derived from Octagonal Symmetry Elements Arising in B-Mn Crystallization of a Simple Monatomic Liquid. Phys. Rev. B **2009**, 79, 144201.

(34) De Graaf, J.; van Roij, R.; Dijkstra, M. Dense Regular Packings of Irregular Nonconvex Particles. Phys. Rev. Lett. **2011**, 107, 1–5.

(35) Haji-Akbari, A.; Engel, M.; Glotzer, S. C. Phase Diagram of Hard Tetrahedra. J. Chem. Phys. **2011**, 135, 194101.

(36) Polya, G. Induction and Analogy in Mathematics; Princeton University Press: Princeton, 1954.

(37) Miller, W. L.; Cacciuto, A. On the Phase Behavior of Hard Aspherical Particles. J. Chem. Phys. **2010**, 133, 234903.

(38) Nezbeda, I. Virial Expansion and an Improved Equation of State for the Hard Convex Molecule System. Chem. Phys. Lett. **1976**, 41, 55–58.

(39) Rohrer, G. S. Structure and Bonding in Crystalline Materials; Cambridge University Press, 2004.

(40) Israelachvili, J. N. Intermolecular and Surface Forces; Academic Press, 2010.

(41) Woodley, S. M.; Catlow, R. Crystal Structure Prediction from First Principles. Nat. Mater. **2008**, 7, 937–946.

(42) Johnson, N. W. Convex Polyhedra with Regular Faces. Can. J. Math. **1966**, 18, 169–200.

(43) Gilbert, E. G.; Johnson, D. W.; Keerthi, S. S. A Fast Procedure for Computing the Distance between Complex Objects in Three-Dimensional Space. IEEE J. Robot. Autom. **1988**, 4, 193–203.

Chapter 5

Self-Assembly of Chiral Crystals[††]

> *If 'shadow life' uses amino acids and sugars, there is a chance*
> *that these will have the reversed chiral signature of familiar standard*
> *life. If so, then extant 'mirror microbes' might be identified by*
> *experimenting with a culture medium of opposite chirality.*
>
> **Paul Davies**

Self-assembly strategies allowing for the crystallization of three-dimensional structures with desired handedness have become increasingly important as a way to generate materials with extraordinary optical activity via a scalable, high yield, process[1]. Recent advances in this direction are mainly restricted to 2D assemblies: anisotropic interactions arising from truncated tips of semiconductor tetrahedra, for instance, lead to the self-assembly of twisted ribbons with an equal distribution of left and right helices[2]; in excluded volume systems, local chiral symmetry breaking has been shown to happen in systems of hard triangular platelets[3]; and computational simulation studies have shown that judicious design of a pair potential can lead to the assembly of target two-dimensional crystals which included a chiral Archimedean tiling[4]. In 3-dimensions, early simulations by Zetterling[5] demonstrated - yet did not explicitly recognize - the assembly of the chiral structure β-Mn from spheres interacting via an isotropic oscillatory pair-potential. Incidentally, the same crystal structure was later also discovered to spontaneously assemble in systems of hard, perfect dodecahedra[6], demonstrating for the first time the possibility of assembly of bulk, 3D chiral crystals from non-chiral building blocks, purely

---

from entropy maximization.

In all those examples, however, the utilization of either non-chiral building blocks or non-chiral interactions makes the handedness of the final chiral structure (i.e. chirality bias) completely undefined a priori, commonly resulting in twin crystals containing both chiralities as opposed to desired single-handed enantiopure crystals. In this work, we employ hard polyhedrally shaped chiral building blocks to study their assembly into both biased and unbiased chiral crystals, demonstrating the two last missing routes connecting nano and colloidal building blocks to bulk chiral crystalline assemblies. By rounding the shape responsible for the assembly of the biased crystal, we show how an achiral crystal can be recovered when sufficient particle rounding is employed, an effect that can be reversed if depletants are used to strengthen particle-particle interactions. By doing so, we demonstrate how an external controller can be used to reconfigure an achiral crystal into an enantiopure chiral crystal, also exemplifying the last missing 'reconfigurability' route connecting achiral and biased chiral crystalline structures.

The routes to chirality. Independently of the particular nature of their systems, such as building block size and type, particle-particle interactions, and scale, researchers aiming to self-assemble chiral crystalline structures will follow one of the routes presented in Fig. 5.1: by employing either achiral (Fig. 5.1, top) or chiral (Fig. 5.1, bottom) building blocks, the resulting assembly will either be achiral (Fig. 5.1, pink), unbiased chiral (blue-red) or a biased, enantiopure chiral crystal (blue). In 3-dimensional systems of colloidal and nanoparticle building blocks, examples of all but two of those routes can be readily found in the literature.

The most commonly observed route connects achiral particles to achiral crystals (assembly route A_{aa}). It corresponds, for instance, to the assembly of spheres[7], ellipsoids[8], and many simple shapes such as tetrahedra[6] into crystals such as FCC, nematic liquid crystals, and quasicrystals. Achiral particles can also assemble chiral crystals. In the absence of chiral forces (route A_{au}), the final crystal structure will have its handedness defined at random, as in the example of hard dodecahedra, which assemble the chiral β-Mn structure[6]. If chiral external forces are employed, achiral particles can be made assembled into biased chiral crystals (route A_{ab}), as in the example of[9] where the handedness of CdTe ribbons can be either random[2] or *a priori* defined, with the employment of circularly

polarized light (CPL).

Despite several examples of chiral building blocks assembling chiral 1D and 2D[10] structures, the only route demonstrating assembly of bulk, 3-dimensional crystals from chiral building blocks resulted in assembly of achiral crystals (route A_{ca}). Many examples of this route can be found in[6], where chiral hard polyhedra assembled into achiral plastic crystals. Therefore, the use of chiral building blocks to assemble unbiased (route A_{cu}) or biased (route A_{cb}) bulk 3-dimensional chiral crystals has, to our knowledge, not been previously demonstrated.

Once the crystalline phase is assembled by one of the routes mentioned above, one interesting possibility of practical importance regards the ability to reconfigure crystals between chirality classes using an external potential, field or parameter. Route R_{au} corresponds to reconfiguration between achiral and unbiased chiral lattices, as observed recently in systems of hard triangles, where chirality spontaneously emerge when extremely high densities are achieved[11]. Route R_{ub} corresponds to reconfiguration between lattices with and without *a priori* choice of chirality, as in the case mentioned above of ribbons of CdTe nanoparticles for which the chirality biasing can be turned on by the presence of CPL[9]. A method able to trigger transformations between bulk achiral and biased chiral structures (Route R_{ab}), as well as examples for the two missing assembly routes above (A_{cu} and A_{cb}), will be discussed in the following section.

The missing assembly routes. In order to demonstrate the assembly of chiral building blocks into chiral crystals with and without chirality bias, we design hard polyhedral particles that can self-assemble into crystalline arrangements via entropy maximization[12–14]. This ability can be understood as a result of effective directional entropic forces between the particles[15], resulting in the formation of highly directional, "covalent" bonding as particle asphericity becomes more and more pronounced. The choice for those building blocks, therefore, is due to their versatile ability to imitate, with some limitations, the complexity of atomistic interactions and assemble a variety of crystal structures[6].

If faces can be used to induce 'covalent-like' bonding between polyhedral particles, the task of designing building blocks able to assemble chiral crystals becomes that of designing shapes that maximize entropic forces when particles are found in the

target, desired crystal. One approach to do so is to construct 'Voronoi particles' (VPs)[16], polyhedra whose shapes are identical to the Voronoi cells of the target crystal and whose assembly at infinite pressure is, by construction, guaranteed to be the target desired structure. An extensive recent study of VPs demonstrated that such an approach is generally successful if two conditions are satisfied: i) the unit cell of the target crystal is small, and ii) the Voronoi particles are sufficiently symmetric and of intermediate sphericity. If those pre-requisites are not satisfied, one usual outcome is the formation of plastic and/or degenerate crystals where the crystalline lattice is assembled but specific contacts between the building blocks are not satisfied.

Armed with this approach, we choose two chiral crystals as targets for our assembly routes. The first is the crystal structure β-Mn. With 20 particles in the unit cell, this Frank-Kasper chiral crystal was recently found to self-assemble from non-chiral dodecahedrally shaped building blocks[6], as well as from spheres interacting via an isotropic pair potential[5]. Given the high coordination number of particles in this crystal (CN = 12), the Voronoi particle is expected to have high sphericity, resulting in a small effect of its chirality on the assembly of the final crystal. This fact, together with the fact that even achiral shapes are able to assemble such a crystal, make those VPs great candidates for assembly of an unbiased chiral crystal via route A_{cu}.

For the second missing route, however, we need a chiral crystal for which strong directional entropic forces between its VPs would lead to biasing of the crystal's chirality. In a recent investigation[17], it was discovered that a system of spheres interacting via a simple, isotropic, medium-ranged oscillatory pair-potential (OPP) could, under the choice of different parameters, self-assemble highly complex structures including a family of icosahedral quasicrystals, clathrates, Frank-Kasper phases, as well as a new cubic chiral crystal. Having only four particles in its unit cell (Fig. 5.1a), this latter structure comprises the simplest possible cubic chiral crystal, yet has the rare space group $P4_132$ which, to date, has never been observed in natural or artificial structures. The low coordination number of particles in this crystal (CN = 6) makes this structure ideal for testing route **A**, because the VP will be, in this case, significantly aspherical Fig. 5.2b.

With our target structure in hand, we analytically construct the perfect crystalline structures and Voronoi cells for both β-Mn and $P4_132$. β-Mn has two different Wyckoff

sites and therefore two different VPs in its lattice (Fig. 5.2a). In contrast, P4$_1$32 has a unique Wyckoff position and its unit cell is composed of four identical (but rotated) polyhedra (Fig. 5.2b). The three VPs have sphericities IQ = insert IQ value here, which suggests that a rotator crystal should be formed in the first system whereas a covalently-bonded crystal should be formed for the later[6].

To investigate the assembly propensity of the VPs, we employ Monte Carlo simulations as in [15]. Simulations were performed in a NVT ensemble with systems of 2048 particles thermalized, by letting the system equilibrate at different packing fractions ranging from $\Phi = 0.50$ to $\Phi = 0.70$. The structure identification was made possible by calculating diffraction patterns and bond order diagrams (see supplementary information of [6] for details).

Results from these MC simulations confirm our expectations. For systems of β-Mn Voronoi particles, we observe that, for density above 58%, systems crystallize into the target lattice. Given the extreme sphericity of the particles, we observe that: i) the chirality of the observed crystal is independent of the chirality of the building block; and ii) particles do not 'lock' into their ideal lattice sites, i.e., both types of Voronoi particles are found randomly placed at different lattice sites. For systems of P4$_1$32 VPs, the low sphericity of the building blocks warrants face-to-face registry and the target chiral lattice, when densities higher than 60% are achieved, are found to assemble always with the same handedness that of the building block. The assembly of plastic and "covalent" chiral crystals described here represent examples of the two missing assembly routes presented in Fig. 5.1. In the next section we examine the possibility of a reconfigurability route connecting the biased chiral and achiral crystal lattices.

The missing reconfigurability route. From the biased chiral crystal assembled above, we set out to investigate the possibility of assembling an achiral crystal from a similar shape as well as the possibility of reconfiguring one crystal into the other. We do so by first rounding each shape - thereby decreasing the strength of the directional entropic forces between particles[15,18,19] - and then studying their assembly behavior. This strategy was demonstrated to allow otherwise facetted shapes to assemble rotator crystals with weakened face-to-face contacts[20,21]. Fig. 5.3 shows the resulting phase diagram of rounded P4$_1$32 VPs as a function of the particle sphericity as measured by their isoperimetric

quotient[6]. The y-axis shows the packing fraction at which simulations were run. We find that as particles become less facetted, a higher packing fraction is needed to ensure face-to-face registry and, therefore, assembly into the biased chiral crystal. All assembled systems were found to have the same chirality as the building block, indicating that weakening DEFs, in this case, leads to destabilization of the chiral crystal phase before it destabilizes the handedness bias. For sufficiently spherical shapes, the systems are found to assemble rotator, achiral BCC and, subsequently, FCC phases.

The assembly of an achiral crystal from a rounded chiral building block offers the interesting possibility of achieving the missing reconfigurability route (**R$_{a-b}$**): if an external parameter can be used to tune the face-to-face interaction between particles, the assembly of either a chiral or biased chiral crystal could be toggled at will. A good choice for such an external parameter is the use of depletants: non-adsorbing macromolecules capable of increasing entropic forces between sufficiently close particles[22], due to the volume between particles excluded to the presence of those macromolecules. Depletants are commonly used to induce attraction between nano and colloidal particles[23] and even employed as a knob for tuning crystalline interparticle distances[24]. In order to simulate systems with depletion, we use a recently developed algorithm[25] that connects a hard particle system to an external reservoir of penetrable hard sphere depletants[26]. With this method, trial moves determine the amount of free volume available to depletants by randomly inserting depletants within the local volume of the trial move and use that value to update the positions of the polyhedral particles.

Fig. 5.3b shows a representation of what we observe in simulations of systems of round VPs in the absence and presence of depletants. By employing a high concentration of depletants (the volume fraction of depletants in the reservoir is 20%, and each depletant has a radius equal to 10% of the chiral particle's circumsphere), VPs that were previously assembling achiral BCC lattices can be made to instead assemble the chiral crystal structure with the same chirality handedness as the building block. This result reveals how the missing reconfigurability route, connecting achiral and biased chiral crystals, can be achieved via control of an external parameter.

Understanding the effects of DEF for chirality bias. In the remaining part of this chapter we discuss the generalities of the proposed directional entropic force approach for

the assembly of chiral crystals from chiral building blocks. The key insight provided by our work is that changes in particle geometry (and therefore particle-particle interaction strength and directionality) allow all instances of chirality assembly routes to be achieved. It is instructive, therefore, to investigate how those two variables (namely interaction strength and directionality) affect the formation of different types of crystals.

In Fig. 5.4, potential of mean force and torque diagrams[18] are shown for different systems of polyhedral particles in the dense fluid (left) and crystalline (middle) configuration. On the right, a representative snapshot of local particle configurations in the crystalline arrangement is shown. Colors represent the relative strength of the directional entropic forces leading to assembly[18,19]. As it can be seen, systems that form biased chiral crystalline structures (Fig. 5.4a, 5.4c) have chiral interactions that greatly exceed those of systems assembling both achiral (Fig. 5.4b) and unbiased chiral (Fig. 5.4d, 5.4e) crystals. The conclusion is that, in order to successfully self-assemble a crystalline structure with chirality imposed by the building block, a significantly strong particle-particle interaction (here, over $5K_BT$) has to be achieved - if not from the shape itself, via additional control such as the presence of depletants.

In summary, we have demonstrated how the last two missing routes for self-assembly of 3-dimensional chiral crystals from nano and colloidal building blocks can be achieved using directional entropic forces. We have shown that a significant strength is required, in those forces, in order to guarantee the assembly of biased chiral crystals, when compared to unbiased and achiral ones. Finally, we have also shown how depletants can be used, in a system of sufficiently spherical particles, to promote reconfigurable assembly between achiral and chiral crystalline arrangements, whose chirality is dictated by that of the building blocks. Our results push the envelope towards the design of a new class of materials whose properties can be tuned at will.
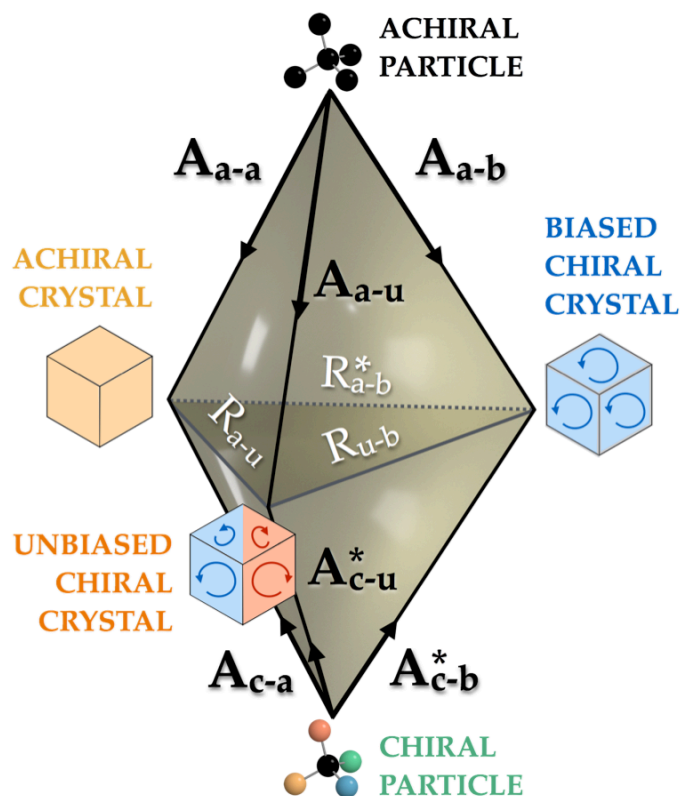
Figure 5.1. The route to chirality. Achiral (top) and chiral (bottom) nano and colloidal particles can assemble three different crystal classes: achiral (pink), unbiased chiral (blue-red) and biased chiral (blue). Unbiased chiral crystals correspond to those whose handedness can not be guaranteed *a priori*. Specific assembly routes (A_{i-j}) connecting particle type i and crystal type j are indicated by directed edges. Once a crystal is assembled, external factors can be used to toggle systems between different crystal classes through reconfigurability routes marked by undirected edges R_{i-j}. Examples for each assembly and reconfigurability route, when existent, are given in the text. Routes marked with * are being reported for the first time in this work.
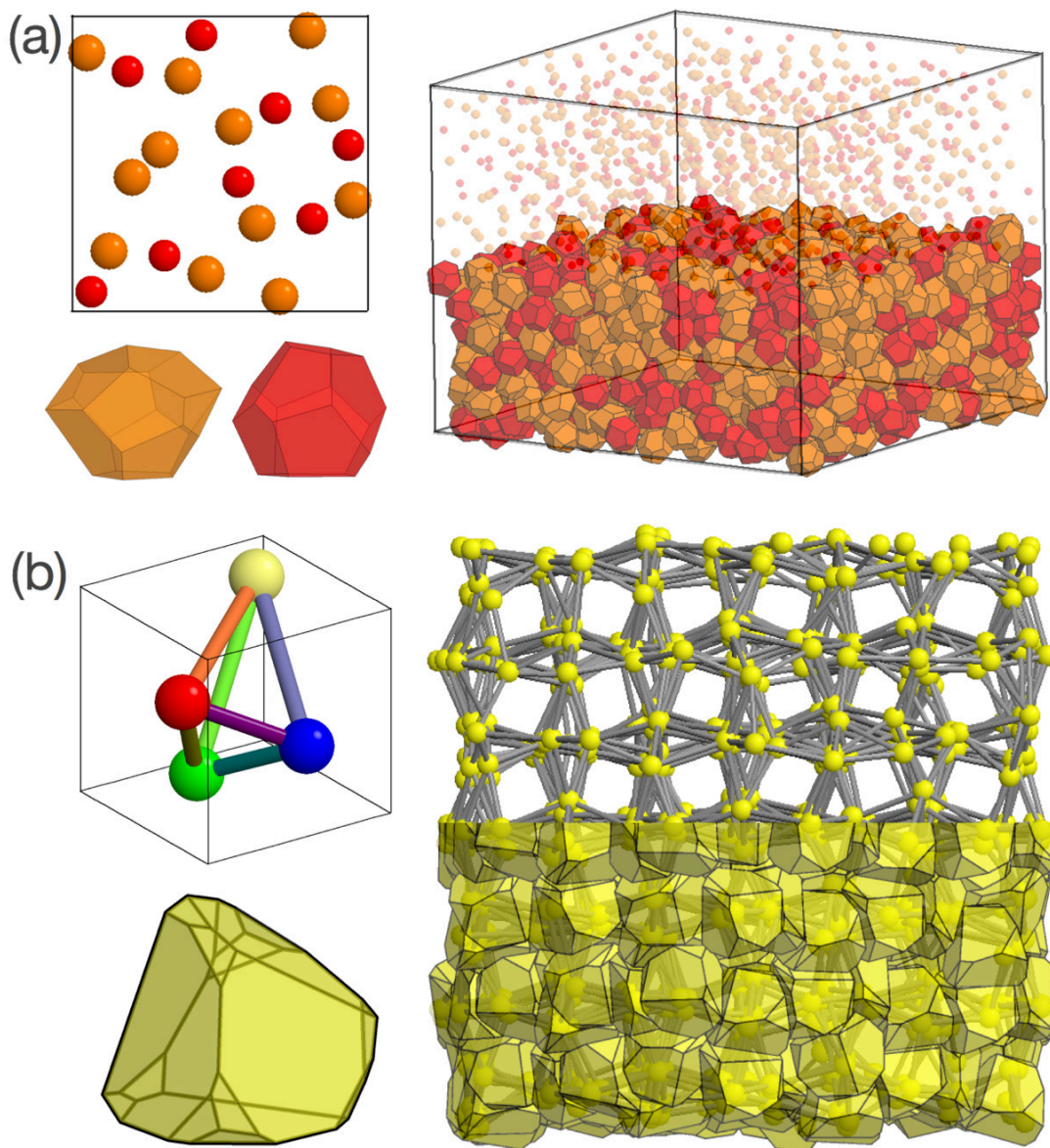
Figure 5.2. Assembly of chiral crystal structures. The unit cell (top left), Voronoi particle (bottom left) and assembled crystal structure (right) for the β-Mn (a) and P4₁32 (b) crystal structures. Interestingly, the assembled β-Mn crystal is compositimally degenerate: any of the two Voronoi particles can be found at a given lattice point. In the P4₁32 structure (b), the chiral square spirals are visible from the assembled crystal.
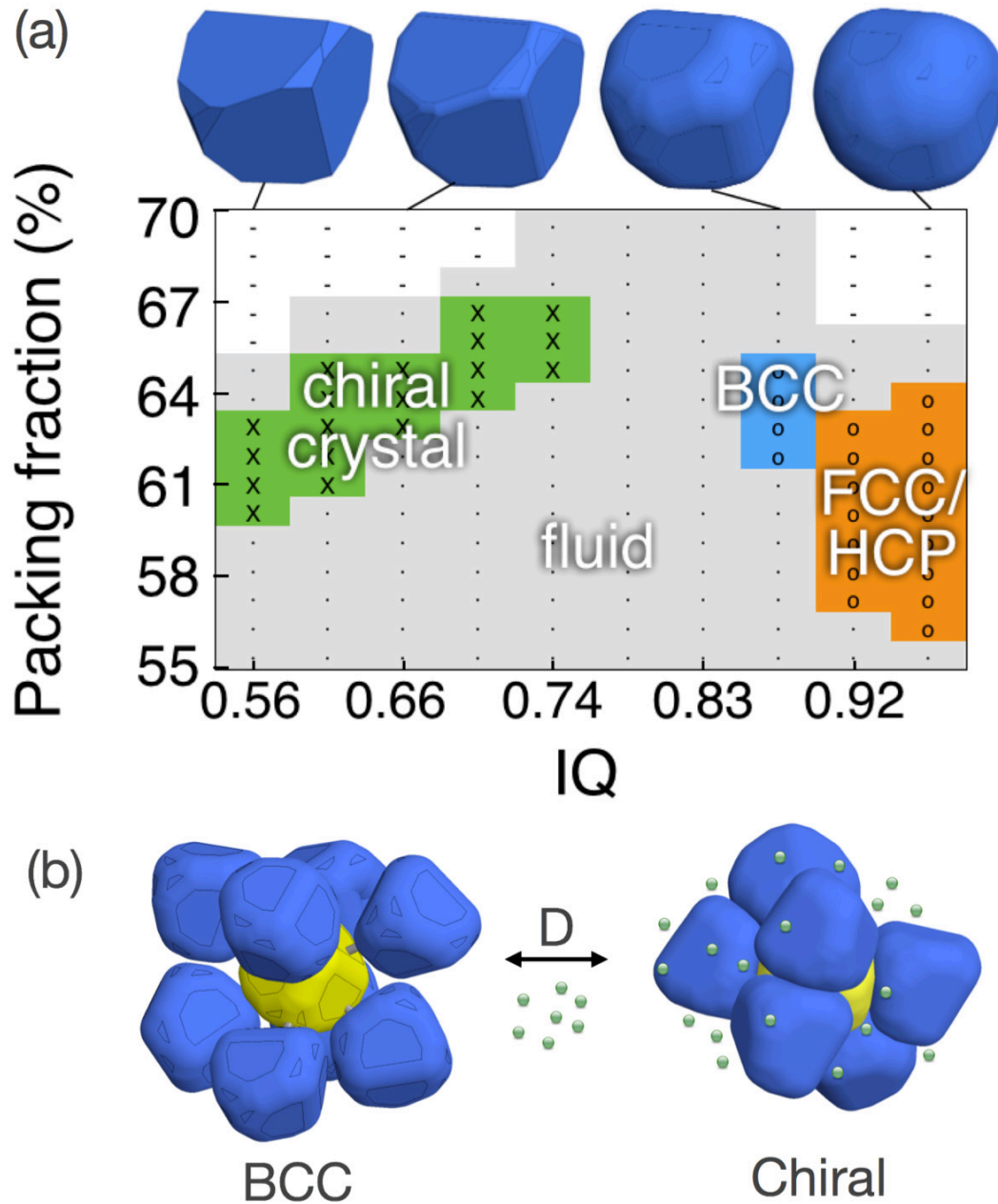
Figure 5.3. Phase diagram for rounded Voronoi particles. (a) The Voronoi particle of P4$_1$32 assembles several crystals as it is made more spherical: from the original chiral crystal to BCC and, finally, FCC. (b) An example of crystal reconfigurability between achiral and chiral crystals can be achieved by adding depletants to a system of very rounded Voronoi particles. At sufficiently high concentration of depletants, a system that would assemble an achiral BCC crystal (b, left) assembles a P4$_1$32 structure with the same handedness as the building block.
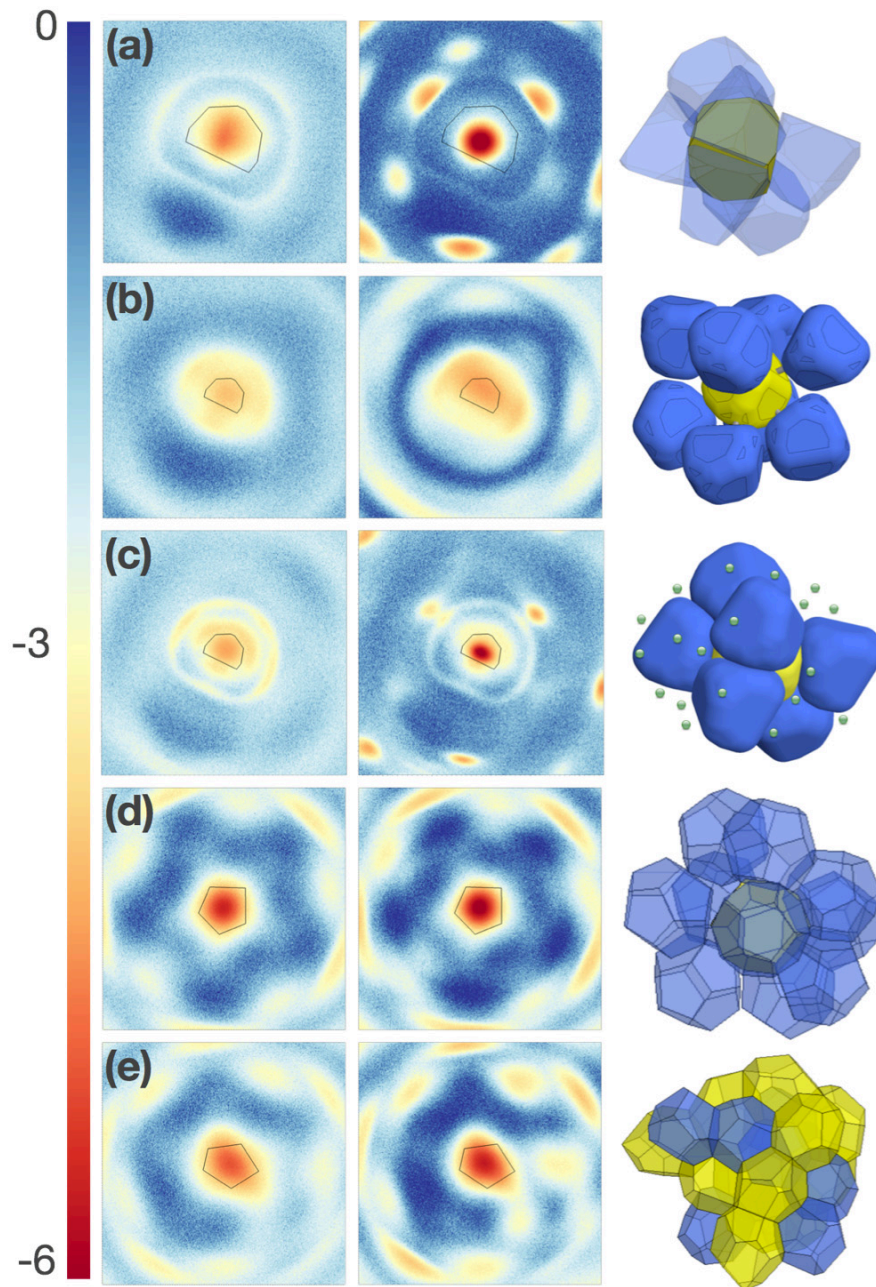
Figure 5.4. Potential of mean force and torque diagrams for different systems of polyhedral particles. Both the dense fluid (left) and crystalline (middle) conditions are shown for: (a) an unmodified $P4_132$ Voronoi particle; (b) a rounded $P4_132$ VP; (c) a rounded $P4_132$ VP with depletants; (d) a dodecahedron forming β-Mn; (e) a β-Mn VP assembling its crystal structure.

References for Chapter 5

(1)   Soukoulis, C. M.; Wegener, M. Past Achievements and Future Challenges in the Development of Three-Dimensional Photonic Metamaterials. *Nat. Photonics* **2011**, *5*.

(2)   Srivastava, S.; Santos, A.; Critchley, K.; Kim, K.-S.; Podsiadlo, P.; Sun, K.; Lee, J.; Xu, C.; Lilly, G. D.; Glotzer, S. C.; *et al.* Light-Controlled Self-Assembly of Semiconductor Nanoparticles into Twisted Ribbons. *Science (80-.).* **2010**, *327*, 1355–1359.

(3)   Zhao, K.; Bruinsma, R.; Mason, T. G. Local Chiral Symmetry Breaking in Triatic Liquid Crystals. *Nat. Commun.* **2012**, *3*, 801.

(4)   Edlund, E.; Lindgren, O.; Jacobi, M. N. Chiral Surfaces Self-Assembling in One-Component Systems with Isotropic Interactions. *Phys. Rev. Lett.* **2012**, *108*, 165502.

(5)   Zetterling, F. Phase Transformations in Computer Simulated Icosahedrally Ordered Phases, Stockholm, 2003.

(6)   Damasceno, P. F.; Engel, M.; Glotzer, S. C. Predictive Self-Assembly of Polyhedra into Complex Structures. *Science (80-.).* **2012**, *337*, 453–457.

(7)   Cheng, Z.; Russel, W. B.; Chaikin, P. M. Controlled Growth of Hard-Sphere Colloidal Crystals. *Nature* **1999**, *401*, 893–895.

(8)   Donev, A.; Cisse, I.; Sachs, D.; Variano, E. A.; Stillinger, F. H.; Connelly, R.; Torquato, S.; Chaikin, P. M. Improving the Density of Jammed Disordered Packings Using Ellipsoids. *Science (80-.).* **2004**, *303*, 990–993.

(9)   Yeom, J.; Yeom, B.; Chan, H.; Smith, K. W.; Dominguez-Medina, S.; Bahng, J. H.; Zhao, G.; Chang, W.-S.; Chang, S.-J.; Chuvilin, A.; *et al.* Chiral Templating of Self-Assembling Nanostructures by Circularly Polarized Light. *Nat. Mater.* **2015**, *14*, 66–72.

(10)   Fejer, S. N.; Chakrabarti, D.; Wales, D. J. Emergent Complexity from Simple Anisotropic Building Blocks: Shells, Tubes, and Spirals. *ACS Nano* **2010**, *4*, 219–228.

(11)   Gantapara, A. P.; Qi, W.; Dijkstra, M. A Novel Chiral Phase of Achiral Hard Triangles and an Entropy-Driven Demixing of Enantiomers. *Arxiv Prepr. arXiv1504.03130v1* **2015**.

(12)   Frenkel, D. Entropy-Driven Phase Transitions. *Phys. A Stat. Mech. its Appl.* **1999**, *263*, 26–38.

(13)   Agarwal, U.; Escobedo, F. A. Mesophase Behaviour of Polyhedral Particles. *Nat. Mater.* **2011**, *10*, 230–235.

(14)   Henzie, J.; Grünwald, M.; Widmer-Cooper, A.; Geissler, P. L.; Yang, P. Self-Assembly of Uniform Polyhedral Silver Nanocrystals into Densest Packings and Exotic Superlattices. *Nat. Mater.* **2012**, *11*, 131–137.

(15)   Damasceno, P. F.; Engel, M.; Glotzer, S. C. Crystalline Assemblies and Densest Packings of a Family of Truncated Tetrahedra and the Role of Directional Entropic Forces. *ACS Nano* **2011**, *6*, 23.

(16)   Schultz, B. A.; Damasceno, P. F.; Engel, M.; Glotzer, S. C. Symmetry Considerations for the Targeted Assembly of Entropically Stabilized Colloidal Crystals via Voronoi Particles. *ACS* **2015**, *9*, 2336–2344.

(17) Engel, M.; Damasceno, P. F.; Phillips, C. L.; Glotzer, S. C. Computational Self-Assembly of a One-Component Icosahedral Quasicrystal. *Nat. Mater.* **2014**.

(18) Van Anders, G.; Klotsa, D.; Ahmed, N. K.; Engel, M.; Glotzer, S. C. Understanding Shape Entropy through Local Dense Packing. *PNAS* **2014**, *111*, E4812–E4821.

(19) Van Anders, G.; Ahmed, N. K.; Smith, R.; Engel, M.; Glotzer, S. C. Entropically Patchy Particles: Engineering Valence through Shape Entropy. *ACS Nano* **2014**, *8*, 931–940.

(20) Ni, R.; Gantapara, A. P.; de Graaf, J.; van Roij, R.; Dijkstra, M. Phase Diagram of Colloidal Hard Superballs: From Cubes via Spheres to Octahedra. *Soft Matter* **2012**.

(21) Zhang, Y.; Lu, F.; van der Lelie, D.; Gang, O. Continuous Phase Transformation in Nanocube Assemblies. *Phys. Rev. Lett.* **2011**, *107*, 2–5.

(22) Asakura, S.; Oosawa, F. On Interaction between Two Bodies Immersed in a Solution of Macromolecules. *Chem. Phys.* **1954**, 1255–1256.

(23) Rossi, L.; Soni, V.; Ashton, D. J.; Pine, D. J.; Philipse, A. P.; Chaikin, P. M.; Dijkstra, M.; Sacanna, S.; Irvine, W. T. M. Shape-Sensitive Crystallization in Colloidal Superball Fluids. *Proc. Natl. Acad. Sci.* **2015**, 201415467.

(24) Young, K. L.; Personick, M. L.; Engel, M.; Damasceno, P. F.; Barnaby, S. N.; Bleher, R.; Li, T.; Glotzer, S. C.; Lee, B.; Mirkin, C. a. A Directional Entropic Force Approach to Assemble Anisotropic Nanoparticles into Superlattices. *Angew. Chemie - Int. Ed.* **2013**, *52*, 13980–13984.

(25) Glasser, J.; Karas, A.; Glotzer, S. C. An Implicit Depletion Method for Hard Particle Monte Carlo. *preprint*.

(26) Lekkerkerker, H. N. W.; Tuinier, R. *Colloids and the Depletion Interaction*; Springer Science & Business Media, 2011; Vol. 833.

Chapter 6

Conclusion and Outlook

Understanding life requires knowledge of how the design of living creatures and emergent phenomena, appearing spontaneously in self-ordered, reproducing, interacting, energy-consuming, non-linear, dynamic ensembles makes us what we are. I believe this will be the next biological revolution.
Peter T. Macklem

In this dissertation I have studied systems of convex Brownian particles interacting only via their inability to occupy the same volume simultaneously. I have done so by both exploring the role played by building block shape on their assembly, and by exploiting general rules – uncovered from these exploratory studies – to design systems capable of assembling target patterns of interest. In what follows, I highlight the scope and main conclusions from each of the three main chapters forming this dissertation.

In the first of these studies[1], the shape of a tetrahedron was systematically truncated and the particles' assembly behavior examined as a function of this shape perturbation. Three major discoveries were made as a result of this study: firstly, shape modifications in the form of vertex truncations were found to lead to the assembly of several new crystal structures, suggesting that faceting alone could lead to the formation of many more complex structures than previously recognized; secondly, it was found that particles in the assembled crystals showed predominantly face-to-face contacts, suggesting the existence of a collective, probabilistic particle-particle influence – which we named directional entropic force (DEF) – dictating the local organization of particles into to their crystalline organization; and finally, it was also found that significant differences could be seen between the structures of the self-assembled crystals and that of the calculated densest packings for each shape, revealing an intrinsic difference between these two optimization problems.

The second paper[2] investigated the generality of the principles uncovered in the previous work. By examining the phase behavior of a diverse set of 145 convex polyhedra and classifying their assemblies according to the symmetry breaking leading to their organization, the main conclusion from this work was that the amount of particle faceting, as measured by the ratio between the particle's surface area and volume, was a good indicator of the magnitude of directional entropic forces between neighboring particles. This recognition – that particle faceting and local organization were correlated – allowed for the development of a framework able to predict the class of crystal structures to be expected from characteristics present in the building block alone, creating there first roadmap for assembly of anisotropic Brownian building blocks into specific classes of patterns.

An interesting corollary from this work was that building blocks could be designed so that the size and location of their facets would lead to the assembly of a particular crystalline structure. This design strategy was later investigated by Schultz et al[3], demonstrating that several target phases could be obtained when judiciously tailored building blocks (whose shapes were identical to that of the Voronoi particle of the crystal being targeted) were constructed. Further studies of – and a framework for quantifying – directional entropic forces were subsequently studies by van Anders et al[4,5].

Finally, the third of the works included in this thesis[6] makes use of the previously referred "Voronoi" strategy of building block design to generate shapes able to assemble 3-dimensional bulk chiral crystalline structures. The main conclusions from this work were that: i) particle faceting will have little contribution for the assembly of chiral crystalline structures with high coordination number and, in those cases, even if the particle used is chiral, the handedness of the final structure cannot be guaranteed *a priori*; ii) particle faceting will be, on the other hand, essential for the assembly process if the chiral crystal has low coordination number, and the final crystal is guaranteed to have the same handedness of the used building block; iii) decreasing the direction of entropic forces in a shape by making it more spherical can lead to the formation of achiral crystals even from chiral building blocks. The assembly of a chiral crystal can be achieved from those shapes by using depletants to increase the strength of DEFs. Together, these results show how shape can be designed for assembly of 3-dimensional chiral crystals with and without *a*

priori control over the chirality handedness. They also demonstrate a reconfigurable path for toggling between achiral and chiral crystals via control of an external parameter.

Altogether, the computational experiments presented here demonstrate how the use of geometrical shapes as building blocks for self-assembly can lead to a variety of novel patterns. The formation of such patterns can be well understood, and even predicted, in light of the proposed concept of directional entropic forces. As a consequence, target structures can be assembled, allowing researchers to tailor the properties of a crystal from the nano-architecture of its building blocks.

The works presented here have been validated both theoretically and experimentally. From the theoretical side, potential of mean force and torque maps were developed to quantify the strength of particle-particle directional entropic forces, revealing that face-to-face configurations are highly favored when particles are sufficiently facetted[4]. From the experimental side, experiments[7–9] have demonstrated the assembly of facetted shapes into crystalline structures in concordance with the *roadmap* presented in chapter 3. The challenges associated with designing more complex building blocks while keeping polydispersity low and the effects of other particle-particle interactions shielded have, so far, kept the most exciting assemblies from being experimentally achieved, holding the gratification of such discoveries for the exciting years to come.

I have also done many related works that were NOT explicitly included in this thesis. In what follows, I overview the findings of those whose central point is within the scope of shape and geometry:

1. "Bad packers" and the Ulam barrier. Why are all known densest packings of 3D convex objects higher than spheres, whereas the equivalent conjecture is not valid in other dimensions? Can we design a shape whose densest packing is worse than spheres by mimicking known 2D "bad packers"? In collaboration with Ruggero Gabbrielli, from the University of Trento, we designed several chiral shapes able to achieve surprisingly low values for their densest packings. Although none of them packed worse than spheres, a very large number of simulations got trapped into sub-optimal, local minima packings, suggesting that the closer you get to finding shapes packing worse than spheres, the harder it will be, from an optimization point of view, to identify this solution. This

unexpected result could have important implications for our understanding of packing landscapes in 3D. (Damasceno, Gabbrielli, and Glotzer, manuscript in preparation).

2. Pair potentials *versus* shapes. An interesting relationship between isotropic pair potentials and hard polyhedra seems to exist: the very same two Frank-Kasper phases found to self-assemble in systems of hard dodecahedra are also observed to assemble from spheres interacting via an isotropic pair potential whose functional form greatly resembles the potential of mean force of systems of dodecahedra. To better investigate those relations, we teamed with Carolyn Phillips, from Argonne NL, to elucidate what kinds of crystal structures could be achieved from oscillatory pair potentials and whether those resembled the crystals assembled from shapes. Indeed, we found that i) a great variety of crystals were found to assemble as a function of the potential parameters; and ii) a large portion of the crystals discovered were also among those crystals assembled from polyhedra. Those results suggest that, indeed, there is a relation between those two distinct classes of systems, one whose details are still being worked out. (Damasceno, Phillips, Engel, Dshemuchadse and Glotzer, manuscript in preparation.)

3. Quasicrystals from isotropic pair potentials. Using potentials of mean force derived from systems of assembled hard truncated tetrahedra, I have investigated the assembly behavior of spheres at different pressures. By modifying the depth of the first well I demonstrated how the inherent local frustration promoted by this pair potential can lead to the assembly of several 3-dimensional quasicrystals, namely: an octagonal, a decagonal, a dodecagonal, and an icosahedral quasicrystal. For the first time one family of pair potentials leads to such a diversity of quasicrystalline structures in 3D, a finding that can help us better understand the hidden relationships between those unusual patterns. (Damasceno, Engel and Glotzer, manuscript in preparation.)

4. Shape for self-replication. Self-replication is a fundamental mechanism for life. The development of simplified models able to provide intuition on its detailed functionality can provide important steps towards its bottom-up imitation in

artificial colloidal systems. So far, the effect of shape has not been explored for self-replication beyond early work by Penrose and Penrose. In order to investigate whether shape can be a useful knob for self-replication, Paul Dodd and I designed lock-and-key shapes that, only due to their shape, will largely prefer to assemble their complementary shapes. With that we were able to demonstrate exponential self-replication of 1-dimensional strings and, in addition, unexpectedly mutate into larger components emerging from their shape complementary. The possibility of using that mechanism for selection of specific features is under investigation. (Damasceno, Dodd and Glotzer, manuscript in preparation.)

Some open questions:

1. Can a MC protocol find the densest packing for a space-filling tetrahedron with 6 particles in the unit cell? What about 24? There are several interesting irregular tetrahedra that are able to completely tile space[10]. Disturbingly, all of the algorithms and protocols described in this dissertation bring the simulations nowhere close to those maximum packing values that are known. Is there a better method for finding those packings? Can the landscape be explored differently? Would the results discovered for more symmetric shapes change and even denser packings be found?

2. How much do atoms behave like shapes? Since van't Hoff, it has been known how geometry can help understand the way atoms and molecules behave. But how much further can this analogy be taken? What kinds of crystals can, and cannot, be achieved in purely entropic systems? What kinds of complex interactions can be replaced by "entropic patches", and would that speed calculations up?

3. Can assembly propensity be predicted from building block's shape? While I was able to demonstrate correlations between shape and the *type* of crystal structure to be assembled, it is still not clear how to predict whether a given shape would assemble at all. Advances around this question would greatly assist experimentalists.

4. <u>Information, building block and assembly</u>. The tetrahedron is the simplest of the 3-dimensional solids. Yet it assembles one of the most intricate structures reported to date. Is this building block "simple", from an information standpoint? Is this crystal "complex"? Is there a relation between the complexity of a shape and that of its assembly? How much complexity has to be put into a building block so that it assembles a target structure of given complexity?

Pitfalls, viewpoints and advice. Most of the simulations performed here were simple enough that they can be easily reproduced, once one has the proper codes to i) perform the MC simulations, and ii) properly analyze the results using tools like the ones I described in chapter 2. In what follows I comment on a few important things to be aware of, when performing those kinds of simulations:

1. **System sizes, periodic boundary conditions and that all.** The number of particles chosen here was a compromise between avoiding finite size effects – in which the size of the box imposes constraints that affect the outcome of our simulation – and performance. In self-assembly simulations of 3D systems, we found that a few thousand particles (typically 2000) were enough to give us fast enough results without apparent finite size effects. As it is common, however, any surprising results were carefully tested for simulation artifacts, and bigger systems were used to check the validity of the results. The same can be said about densest packing calculations. However, simulations with more than 4 particles in the unit cell start to become prohibitively expensive and, to date, we still do not know whether denser packings for those shapes can be found if more particles are used in the simulation box. Similarly, simulations with different boundary conditions (PBCs) should be performed when surprising results emerge. <u>A very important open question remains how to perform simulations with PBCs that do not disrupt crystal formation, even if they have unusual symmetries such as that of an icosahedral quasicrystal.</u>

2. **Human time versus computer time.** Even with computation becoming cheaper,

it is still not financially possible to run all the simulations we want and need. Worse than that: even if we could do so, the amount of time needed to analyze such data would surpass the desired length of our doctorate degree. So another balance that has to be found, in addition to the compromise mentioned above between precision and simulation speed, is that of time spent writing a code versus time spent gathering science from it. My approach and suggestion has been to discover, as soon as possible, where do you fit in the "relevant expertise" spectrum and collaborate with people with complementary skills, from whom you can learn while speeding up the process of discovery and reporting. You will have more authors in your papers but on the brighter side you always have someone else to blame if things go wrong.

3. **What is the question.** Perhaps the hardest thing to learn during a research endeavor is how to ask the right questions. Again, as computation becomes cheaper, one is many times tempted to ask questions of the type "what would happen if…?" followed by a number of parameters that could be changed. This exploratory approach is a great way to start doing research, get your "hands dirty" and learn how to use the tools as long as it is fine if no results come out of this. Later on, however, when trying to narrow down a research topic, a more focused approach is needed. In my experience, finding a question that interests you, before anyone else, is the most important step. After that, it is somewhat important to find out i) whether anyone else cares about that question, ii) why it has not been solved before, and iii) what impact can you make. Finally, for every simulation run and every result gathered you should ask: how will they help me getting closer to answering this question? And given the new results that come, what are the next steps that make me get as close as possible to solving the mystery? That might mean breaking your original question into smaller and smaller bits, but that is fine (and usually the way science works). The important part is to learn new things, no matter how specific they are, while still keeping track of the overall motivation, big picture and goal. As a consequence of this procedure, every presentation you will give and every

paper you will write about that research question will become much easier to state and, consequently, to be followed by your audience. For more detailed strategies, Beveridge's "The Art of Scientific Investigation"[11] is a great read. I also recommend chapter 8 of Jesse Schell's book "The Art of Game Design"[12]: just replace the word "game" by "your PhD" and you will do fine.

Outlook. The science of self-assembly will live for as long as science does. This is so because a large part of the natural world, from molecules to galaxies, was formed via self-assembly, and understanding their formation means nothing less than unveiling some of the organizing principles of Nature itself. In finishing this thesis I realize how much the exciting progress in this field is still to come: that arising from integration across length and time scales.

As largely discussed in this thesis, nanoparticles organize themselves into periodic patterns by finding a compromise between their desired disorder and the constraints imposed by their neighborhood. Which other systems can those ideas be stretched to? Which other building blocks, interacting locally or globally, moving in real or some higher dimensional space, are able to form spatial-temporal structures due to the constraints imposed by their environment? I believe many. Understanding the emergence of structure in those systems will depend on a vast expansion of our physics of near-equilibrium conditions towards more complex, dissipative, dynamic – but nonetheless self-organizing – circumstances.

As computation – and data analysis – becomes cheap, the frontier of self-assembly studies will be to identify structures emerging on longer time scales and only as a result of multiple types of "alive" building blocks, helping, constraining, competing and even modifying each other in crowded, living-like environments.

In other words, to get a breadth on how far self-assembly will go one has to look no further than to what Nature has so far achieved.

References for Chapter 6

(1)   Damasceno, P. F.; Engel, M.; Glotzer, S. C. Crystalline Assemblies and Densest Packings of a Family of Truncated Tetrahedra and the Role of Directional Entropic Forces. *ACS Nano* **2011**, *6*, 23.

(2)   Damasceno, P. F.; Engel, M.; Glotzer, S. C. Predictive Self-Assembly of Polyhedra into Complex Structures. *Science (80-.)*. **2012**, *337*, 453–457.

(3)   Schultz, B. A.; Damasceno, P. F.; Engel, M.; Glotzer, S. C. Symmetry Considerations for the Targeted Assembly of Entropically Stabilized Colloidal Crystals via Voronoi Particles. *ACS Nano* **2015**, 150218161039001.

(4)   Van Anders, G.; Klotsa, D.; Ahmed, N. K.; Engel, M.; Glotzer, S. C. Understanding Shape Entropy through Local Dense Packing. *PNAS* **2014**, *111*, E4812–E4821.

(5)   Van Anders, G.; Ahmed, N. K.; Smith, R.; Engel, M.; Glotzer, S. C. Entropically Patchy Particles: Engineering Valence through Shape Entropy. *ACS Nano* **2014**, *8*, 931–940.

(6)   Damasceno, P. F.; Karas, A.; Schultz, B. A.; Engel, M.; Glotzer, S. C. A Directional Entropic Force Approach for Self-Assembly of 3-Dimensional Enantioselective Crystals. *preprint* **2015**, 1–5.

(7)   Young, K. L.; Personick, M. L.; Engel, M.; Damasceno, P. F.; Barnaby, S. N.; Bleher, R.; Li, T.; Glotzer, S. C.; Lee, B.; Mirkin, C. A. A Directional Entropic Force Approach to Assemble Anisotropic Nanoparticles into Superlattices. *Angew. Chemie - Int. Ed.* **2013**, *52*, 13980–13984.

(8)   Zhang, Y.; Lu, F.; van der Lelie, D.; Gang, O. Continuous Phase Transformation in Nanocube Assemblies. *Phys. Rev. Lett.* **2011**, *107*, 2–5.

(9)   Henzie, J.; Grünwald, M.; Widmer-Cooper, A.; Geissler, P. L.; Yang, P. Self-Assembly of Uniform Polyhedral Silver Nanocrystals into Densest Packings and Exotic Superlattices. *Nat. Mater.* **2012**, *11*, 131–137.

(10)   Senechal, M. Which Tetrahedra Fill Space? *Math. Mag.* **1981**, 227–243.

(11)   Beveridge, W. I. B.; *The Art of Scientific Investigation.*; 2nd ed.; Melbourne, London, Toronto: William Heinemann Ltd., 1950.

(12)   Schell, J. *The Art of Game Design*; 2nd ed.; CRC Press, 2011.